https://doi.org/10.5194/essd-2023-389
Preprint. Discussion started: 27 September 2023

Open Access Earth System Science Data Discussions

Systematically tracking the hourly progression of large wildfires using GOES satellite observations

Tianjia Liu[1], James T. Randerson[1], Yang Chen[1], Douglas C. Morton[2], Elizabeth B. Wiggins[3], Padhraic Smyth[4], Efi Foufoula-Georgiou[1], Roy Nadler[5], and Omer Nevo[5]

[1]Department of Earth System Science, University of California, Irvine, Irvine, CA, USA
[2]NASA Goddard Space Flight Center, Greenbelt, MD, USA
[3]NASA Langley Research Center, Hampton, VA, USA
[4]Department of Computer Science, University of California, Irvine, Irvine, CA, USA
[5]Google, 1600 Amphitheater Parkway, Mountain View, CA, USA

Correspondence to: Tianjia Liu (tianjia.liu@uci.edu)

Abstract. In the western United States, prolonged drought, warming climate, and historical fuel build-up have contributed to larger and more intense wildfires, as well as longer fire seasons. As these costly wildfires become more common, new tools and methods are essential for improving our understanding of the evolution of fires and how extreme weather conditions, including heatwaves, windstorms, droughts, and varying levels of active fire suppression, influence fire spread. Here we develop the GOES-Observed Fire Event Representation (GOFER) algorithm to derive the hourly fire progression of large wildfires and create a dataset of hourly fire perimeters, active fire lines, and fire spread rates. Using GOES-East and GOES-West geostationary satellite detections of active fires, we test the GOFER algorithm on 28 large wildfires in California from 2019-2021. The GOFER algorithm includes parameter optimizations for defining the burned-to-unburned boundary and correcting for the parallax effect from elevated terrain. We evaluate GOFER perimeters with using 12-hourly data from the VIIRS-derived Fire Event Data Suite (FEDS) and final fire perimeters from California's Fire and Resource Assessment Program (FRAP). Although the GOES imagery used to derive GOFER has coarser resolution (2 km at the equator), the final fire perimeters from GOFER correspond reasonably well with those obtained from FRAP, with a mean Intersection-over-Union (IoU) of 0.77, in comparison to 0.83 between FEDS and FRAP. GOFER fills a key temporal gap present in other fire tracking products that rely on low-earth-orbit imagery, where perimeters are available at 12-hour intervals or longer, or at ad hoc intervals from aircraft overflights. This is particularly relevant when a fire spreads rapidly, such as at maximum hourly spread rates of over 5 km/h. Our GOFER algorithm for deriving the hourly fire progression using GOES can be applied to large wildfires across North and South America and reveals considerable variability in rates of fire spread on diurnal time scales. The resulting GOFER dataset has a broad set of applications, including the development of predictive models for fire spread and improvement of atmospheric transport models for surface smoke estimates.

1 Introduction

Severe wildfire seasons in the western United States, such as in 2018, 2020, and 2021, generate large negative economic and public health impacts, displacing communities in the wildland-urban interface and inducing hazardous smoke pollution (Burke et al., 2021; Zhou et al., 2021). Following the legacy of total forest fire suppression in the 20th century, the enhanced drying of fuels from anthropogenic climate warming and a lack of prescribed burns for fuel reduction have increased the likelihood of destructive, fast-spreading megafires, such as the Creek Fire in 2020 (1537 km^2) and Dixie Fire in 2021 (3898 km^2) (Juang et al., 2022; Kolden, 2019; Williams et al., 2019). However, these extreme fire events, which are infrequent and outliers in terms of fire size, are often poorly characterized in statistical models of burned area or fire intensity (Joseph et al., 2019; Wang et al., 2021).

https://doi.org/10.5194/essd-2023-389
Preprint. Discussion started: 27 September 2023

As a consequence, it is important that we first understand how large fires evolve through both time and space to sufficiently model how meteorology, suppression, and fuels modulate fire spread and emissions.

Recent efforts to map the progression of fire perimeters include the Global Fire Atlas (Andela et al., 2019), GlobFire (Artés et al., 2019), Fire Events Delineation (FIRED) (Balch et al., 2020), and the Fire Event Data Suite (FEDS) (Chen et al., 2022). These datasets use satellite observations of fires from MODIS or VIIRS, and cluster burned pixels or active fire detections into individual fire events. The Global Fire Atlas, GlobFire, and FIRED use the 500-m MODIS burned area product to map daily fire progression, while FEDS uses the 375-m VIIRS active fire product to map 12-hourly fire progression. The Global Fire Atlas and GlobFire operate on a global scale, while FIRED and FEDS are restricted to a regional level – the contiguous United States for FIRED and California for FEDS.

Here we improve the temporal scale of existing mapping methods for fire perimeters to hourly intervals by leveraging geostationary satellite observations from the GOES-East and GOES-West satellites. Our baseline algorithm is based on Google's initial method used to produce the wildfire layer in Google Maps (Restif and Hoffman, 2020). The wildfire layer, which updates within 30 minutes of GOES retrievals, displays the current perimeter of large fires based on GOES active fire observations and aims to provide stakeholders with up-to-date information on how current fires may endanger nearby structures and lead to evacuations. To create the wildfire layer, Google Maps leverages the Google Earth Engine (GEE) cloud-based geospatial computing platform (Gorelick et al., 2017; Restif and Hoffman, 2020). GEE's petabyte-scale public data catalog maintains the GOES datasets and automatically adds and preprocesses new images as soon as they are available. GEE empowers rapid processing of large amounts of data and enables the tracking of fire progression at high temporal resolution.

In this study, we develop the GOES-Observed Fire Event Representation (GOFER) algorithm to derive the hourly fire progression of large wildfires. Our algorithm includes an optimized threshold for delineating the fire perimeter from unburned areas, parallax terrain correction for GOES images, a dynamic smoothing kernel, and scaling adjustment for early perimeters. As a test case of the GOFER algorithm, we create a dataset that includes hourly fire perimeters, active fire lines, and fire spread rates for large fires that burned over 50,000 acres (202 km^2) in California from 2019-2021. A set of 28 fires met this criterion, including some of the largest (August Complex and Dixie) and most destructive fires (North Complex and Glass) in California's history. Over this 3-year span, these fires approximately accounted for 85% of the total burned area and 77% of all the structures destroyed. We evaluate GOFER perimeters and active fire lines using FEDS at 12-h intervals and validate the spatial accuracy of the final perimeter with FRAP, a fine-resolution dataset of fire perimeters derived from incident reports, remote sensing, and ground surveys. Finally, we discuss the limitations, future development, and applications of the GOFER algorithm and dataset.

2 Data and Methods

2.1 Study region

Table 1: Metadata and GOFER-Combined summary statistics for the 28 large wildfires in California from 2019-2021 over 50,000 acres (202 km^2). The area (km^2) refers to that of the final perimeter. Also shown are the maximum hourly concurrent ($fline_{c=0.05}$) and retrospective ($fline_r$) active fire line lengths, in km, and the fire spread rates, in km/h, calculated from the maximum axis of expansion ($fspread_{MAE}$) and area-weighted expansion methods ($fspread_{AWE}$).

#	Fire Name	Year	Area (km^2)	$fline_{c=0.05}$ (km)	$fline_r$ (km)	$fspread_{MAE}$ (km/h)	$fspread_{AWE}$ (km/h)
1	Kincade	2019	347	45.7	25.3	4.9	2.7
2	Walker		268	62.4	23	5.6	3.2

3	August Complex	2020	4343	210.5	92.2	5.1	1.7
4	Bobcat		584	62.2	34	4.3	1.9
5	Creek		1615	121.7	52.1	11.3	4.2
6	CZU Lightning Complex		283	61.5	37.7	5	1.6
7	Dolan		501	63.1	27.9	3.6	1.9
8	Glass		353	65.5	29.4	7.6	3.5
9	July Complex		171	40.1	27.6	4.6	1.4
10	LNU Lightning Complex (Hennessey)		1539	264	114	10.5	1.8
11	North Complex		1344	126.2	65.6	9.9	3.1
12	Red Salmon Complex		575	59.7	26.4	3.1	1.3
13	SCU Lightning Complex		1526	134.7	62.9	4.8	1.5
14	Slater and Devil		697	113.9	39.1	6	2.9
15	SQF Complex		786	71.4	22.1	5.2	2.8
16	W-5 Cold Springs		364	57.7	22.8	3.5	1.2
17	Zogg		223	49.1	19.1	6.2	10.8
18	Antelope	2021	599	52.9	32.7	4.8	2.3
19	Beckwourth Complex		558	76.3	31.1	4.7	1.7
20	Caldor		994	88.7	42.6	4.3	2.3
21	Dixie		4389	187.1	67.2	10.2	2.9
22	KNP Complex		389	64.2	22.6	2.6	1.6
23	McCash		406	67.7	28.6	2.7	1.5
24	McFarland		567	62.7	30.4	4.1	1.4
25	Monument		925	83.6	41	3.8	1.5
26	River Complex		931	124.2	39.8	5.2	1.5
27	Tamarack		375	64.2	23.7	3.7	3.9
28	Windy		427	64.2	30	2.2	0.9

https://doi.org/10.5194/essd-2023-389
Preprint. Discussion started: 27 September 2023

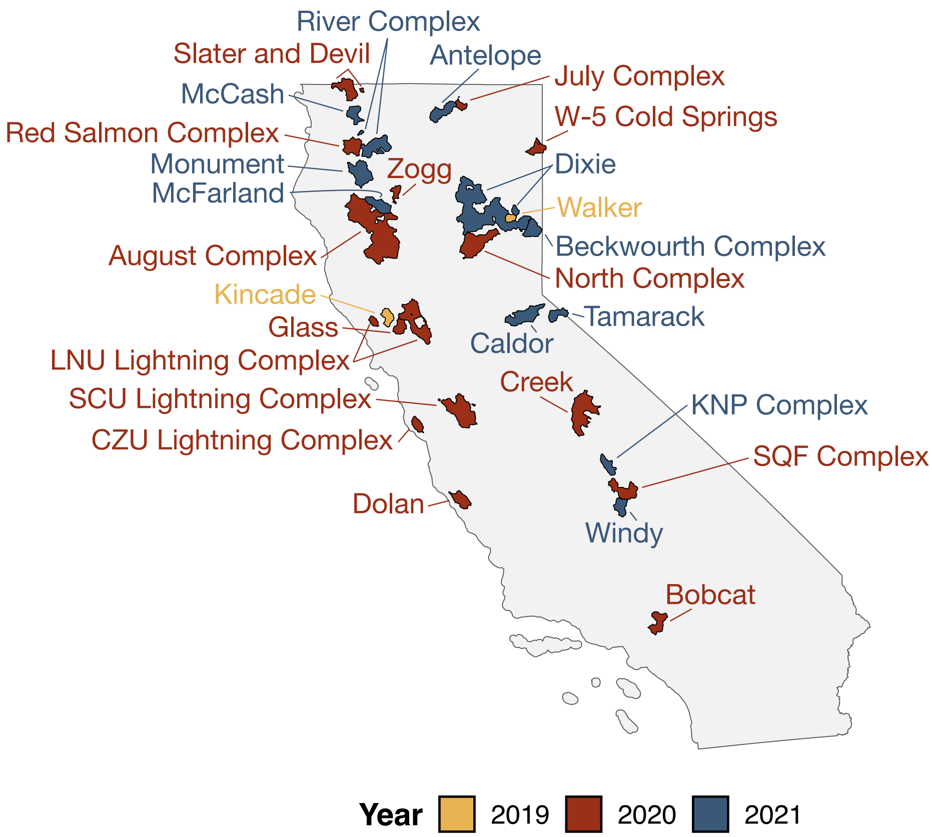

Figure 1: Map of the final perimeters for 28 large fires in California in the GOFER dataset. In total, GOFER contains 2 fires in 2019, 15 fires in 2020, and 11 fires in 2021; all the fires mapped are over 50,000 acres (202 km^2). The footprints of the fires shown are from GOFER-Combined.

We map the hourly progression of 28 large wildfires in California (CA) from 2019-2021 (Tables 1, A1; Figures 1, A1). Here we define a large wildfire as a fire that burns over 50,000 acres (202 km^2). The 28 wildfires include three "cross-border" fires (Slater and Devil, W-5 Cold Springs, and Tamarack) that burned across the California border into neighbor states.

2.2 Datasets

We use active fire detections from the Advanced Baseline Imager (ABI) aboard NOAA's Geostationary Operational Environmental Satellite (GOES)-16/East and 17/West, which observe North and South America with a spatial resolution of 2 km at the equator and temporal resolution of 10-15 minutes for its full disk view (Schmit et al., 2017). The different longitudinal positions of GOES-East (75°W) and GOES-West (137°W) yield views of the same fire from two different perspectives, generating images with two different spatial footprints for a given location. The Level-2 GOES Fire/Hot Spot Characterization product includes information on the data quality of the active fire retrieval ("fire mask categories"), fire temperature, fire area, and fire radiative power (FRP), which is a proxy for fire intensity (Hall et al., 2019; Schroeder et al., 2010; Xu et al., 2010). To correct the terrain-induced parallax displacement in GOES images, we use the USGS 3D elevation program (3DEP) digital elevation model (DEM) at 10-m (1/3 arc second) spatial resolution (Archuleta et al., 2017).

https://doi.org/10.5194/essd-2023-389
Preprint. Discussion started: 27 September 2023

We retrieve the ignition time and location of each fire from the California Department of Forestry and Fire Protection (CAL FIRE; https://www.fire.ca.gov/) and InciWeb, the U.S. interagency all-risk incident information system (https://inciweb.nwcg.gov/). When CAL FIRE does not report detailed information on fires outside of its jurisdiction (i.e., on federal lands), we rely on InciWeb to fill the gap. This metadata is used to check the fire ignition time against the GOES active fire time series and to limit the amount of GOES data spatially and temporally to process and avoid GEE computational limits.

For optimization and validation, we use several datasets derived from higher spatial resolution observations: FEDS, Monitoring Trends in Burn Severity (MTBS), and the Fire and Resource Assessment Program (FRAP). MTBS uses Landsat (30 m) imagery to map the final fire perimeter and burn severity from 1984-present and is available with about a 2-year lag time; MTBS maps all fires over 1000 acres (4 km^2) in the western U.S. (Picotte et al., 2020). FEDS uses object-based tracking of VIIRS active fires (375 m) to map the progression of fires in California at 12-h timesteps from 2012-2021 (Chen et al., 2022). The historical fire perimeters dataset from CAL FIRE's FRAP is the most detailed and complete dataset for California wildfires, which are mapped by GPS and aerial observations (https://frap.fire.ca.gov/). FRAP standardizes and combines perimeters from federal agencies (U.S. Forest Service, Bureau of Land Management, National Park Service, and Fish and Wildlife Service). For select fires (12 of 28 fires), CAL FIRE also provides the location of structures within the perimeter and the level of damage sustained by each structure (accessed from the California Open Data Portal: https://data.ca.gov/). These data are used to calculate the number of affected and destroyed structures contained by our derived fire perimeters.

https://doi.org/10.5194/essd-2023-389
Preprint. Discussion started: 27 September 2023

2.3 Using GOES active fire detections to derive hourly perimeters

2.3.1 Overview of the GOFER algorithm

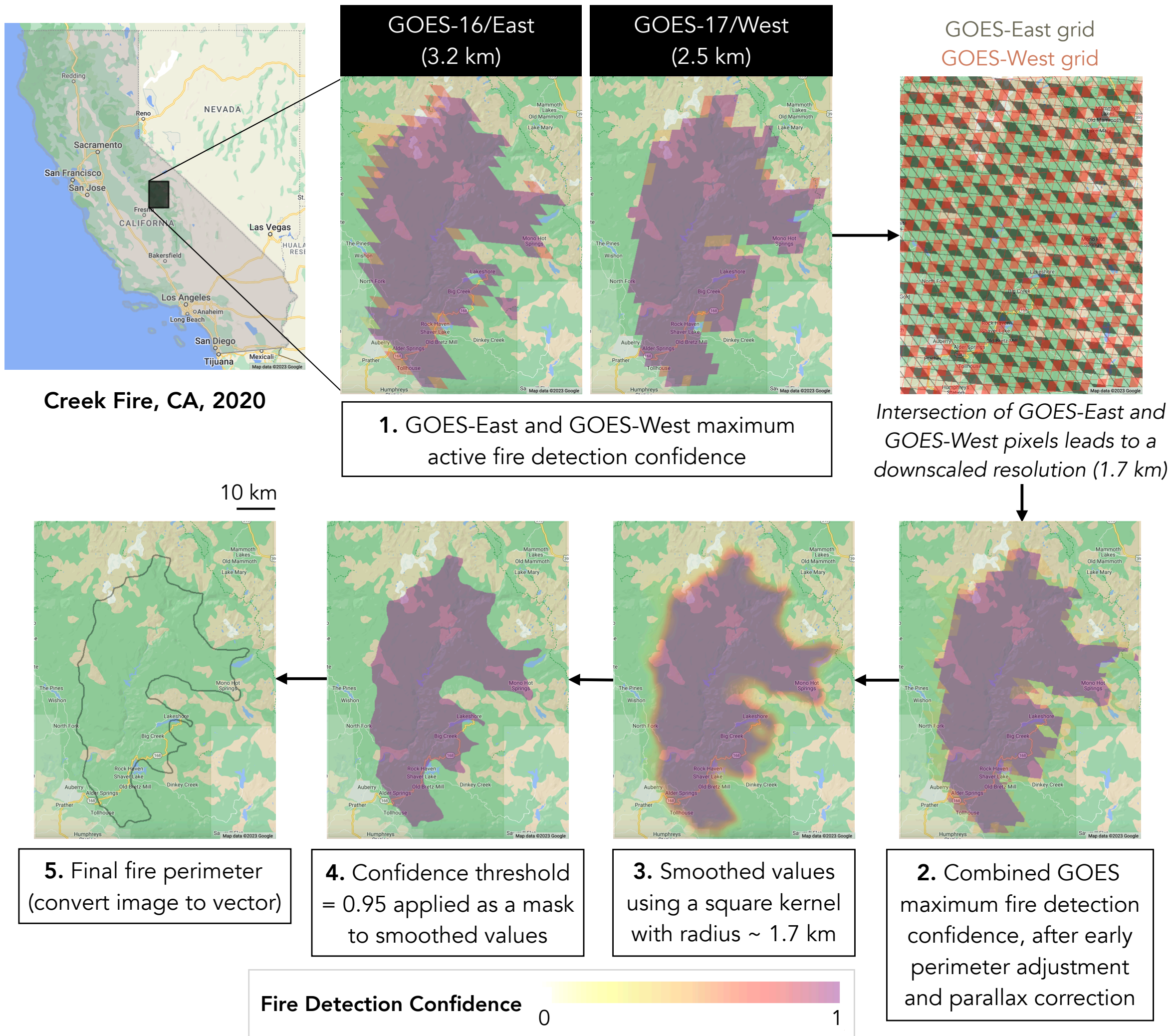

Figure 2: Pictorial depiction of the GOFER workflow used to produce fire perimeters from GOES active fire detections in Google Earth Engine. The gray shaded area represents the state of California, and the black box shows the location of the Creek Fire in 2020. This example shows the workflow for producing the final fire perimeter of the Creek Fire and uses all GOES images from the hour of ignition to the last fire detection. The GOES nominal spatial resolution is 2 km at the equator but varies based on the pixel's location relative to the longitudinal position of the GOES satellite; the GOES resolutions inset are specific to the Creek Fire. The background map data is from ©2023 Google Maps, rendered on Google Earth Engine.

Restif and Hoffman (2020) show a step-by-step example of a GOES-based image-to-vector method to map fire perimeters in GEE. Here we expand and improve this method by adding four optimizations or adjustments in our GOFER algorithm: (1) dynamic smoothing kernel size, (2) early perimeter adjustment, (3) parallax terrain correction, and (4) confidence threshold optimization. As an example, we pictorially depict the steps to produce the final perimeter of the 2020 Creek Fire in Figure 2.

https://doi.org/10.5194/essd-2023-389
Preprint. Discussion started: 27 September 2023

In step 1, we assign GOES-East and GOES-West fire mask codes as fire detection "confidence" values that range from 0 to 1 (Table B1), and for each satellite, calculate the maximum fire detection confidence over the temporal stack of images from ignition to the end hour. For the Creek Fire, the average spatial resolution is about 3.2 km for GOES-East and 2.5 km for GOES-West, calculated from the GOES pixel area within a bounding box covering the fire's extent. Due to the different pixel orientations and resolutions of the GOES-East and GOES-West grids, we overlay them to create a combined grid at a downscaled spatial resolution. The combined grid is heterogenous in pixel size with an area-weighted spatial resolution of 1.7 km. The spatial resolution of the combined grid is later used in step 3 to determine the kernel radius to smooth the fire detection confidence image (Section 2.3.3.1).

In step 2, we apply scaling factors from the early perimeter adjustment to the stack of hourly fire detection confidence images (Section 2.3.3.2). The early perimeter adjustment ensures that perimeters are formed at the start of a fire despite dilution from neighborhood smoothing in step 3 and despite possible absence of high fire confidence pixels to overcome the confidence threshold applied in step 4. We combine the GOES-East and GOES-West maximum fire detection confidence by taking the average. We also correct the terrain-induced parallax displacement in each satellite (Section 2.3.3.3). Due to the elevation and location of the fire relative to the satellite's viewing angle, the GOES-observed fire pixels are displaced from their actual location; displacements are greater for fires at high elevations and located toward the edge of the GOES disk. The early perimeter adjustment and parallax correction are needed steps to improve the temporal and spatial accuracy, respectively, of the perimeter but not accounted for in Restif and Hoffman (2020).

In step 3, we smooth the values using a square kernel with a radius equal to the area-weighted spatial resolution of pixels within the area of interest. Restif and Hoffman (2020) set an arbitrary kernel size of 2 km, whereas our dynamic calculation of the kernel size accounts for the heterogenous pixel size of the combined grid (Section 2.3.3.1). Using the kernel to apply a neighborhood mean, the smoothing transforms the fire detection confidence values into a continuous gradient and removes blockiness at the edges.

In step 4, we apply a threshold mask of 0.95 to the smoothed confidence values. Restif and Hoffman (2020) arbitrarily set the confidence threshold to 0.6, while we optimize for the confidence threshold, as discussed in Section 2.3.3.3. In addition, Restif and Hoffman (2020) use a spatial resolution of 200 m for the intermediate image with the smoothed fire detection. We opt for a higher spatial resolution of 50 m to reduce blockiness at the edges of the polygon formed in step 5. At coarser resolution, the edges of the polygon are more staircase-like, mirroring the pixel edges of the raster.

In step 5, the image is converted to a polygon that represents the fire perimeter. To further smooth the geometric complexity induced by the image-to-vector conversion and reduce the file size of the polygon, we simplify the polygon with a maximum error margin of 100 m, which is in a 2:1 ratio with the spatial resolution of the smoothed confidence image. This ratio is similar to Restif and Hoffman (2020), who set the maximum error margin to 500 m, versus 200 m, for the smoothed fire confidence image.

In addition to the combined GOES method, we also create perimeters and related fire metrics solely using GOES-East imagery or GOES-West imagery to test the efficacy of using just one satellite. We separately optimize the confidence threshold and parallax adjustment factor and calculate the smoothing kernel size and early perimeter adjustment for each GOFER version. Hereafter, we refer to the three GOFER versions as GOFER-Combined, GOFER-East and GOFER-West. For this study, GOFER-Combined uses GOES-16 and GOES-17 observations; GOFER-East uses only GOES-16 observations, and GOFER-West uses only GOES-17 observations. We note that GOES-17 has been replaced by GOES-18 in early 2023.

https://doi.org/10.5194/essd-2023-389
Preprint. Discussion started: 27 September 2023

2.3.2 Pre-processing: Input metadata dictionary

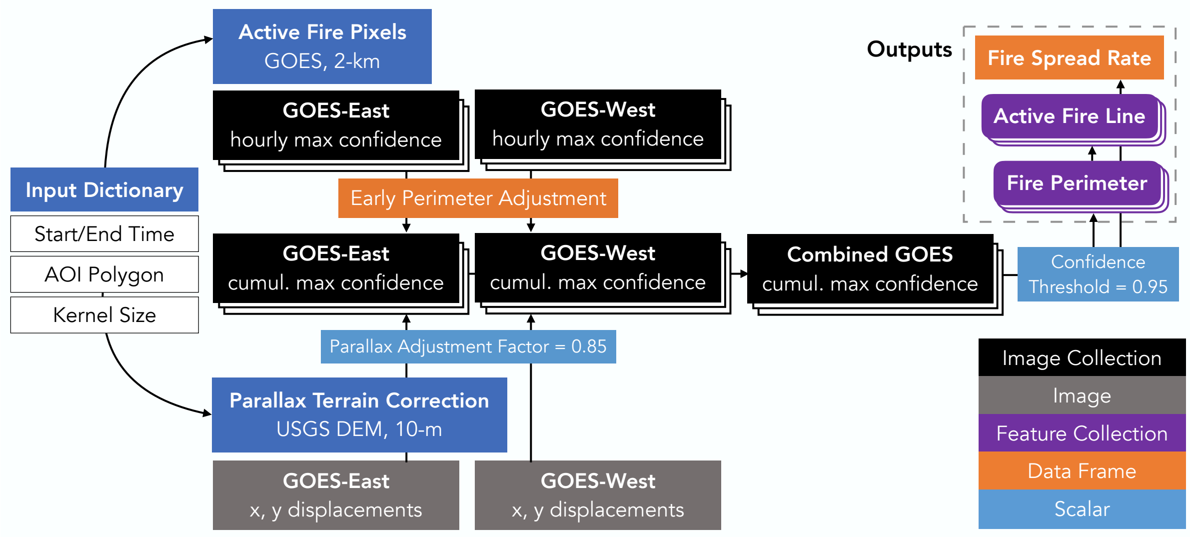

Figure 3: Overview of the GOFER workflow used to produce the GOES-derived fire perimeters and ancillary fire metrics (active fire line and fire spread rate). The confidence threshold and parallax adjustment factor values are optimized using the 10 largest wildfires in California in 2020. The dark blue boxes are headings to denote the different input data.

In the pre-processing stage, we create a dictionary of input values for each fire (Figure 3). In particular, we set temporal and spatial constraints for calculating fire progression, i.e., the start and end time bounds and area of interest (AOI) polygon. For start time, we use the ignition time as reported by CAL FIRE, when possible, or InciWeb and round down by hour (e.g., 6:37 to 6:00). However, GOES can detect active fires prior to the ignition time for some fires – mainly lightning-caused fires; for such cases, we set the hour of the earliest GOES active fire detection as the start time. We set the end time as the hour with the last GOES active fire detection that occurs within a few days of previous detections, provided that the fire has converged to close its final size recorded by CAL FIRE or InciWeb. This is an approximate estimate of the end time, as a later quality control step sets the end hour as when the fire perimeter last expanded (Section 2.3.4). For the AOI polygon, we start with the CAL FIRE or InciWeb ignition coordinates and expand to a simple rectangle or polygon that includes the footprint of GOES active fire detections related only to that fire.

2.3.3 Processing: Development, optimizations, and improvements

In the processing stage, we implement the four optimizations or adjustments in the GOFER fire perimeter mapping method: (1) dynamic smoothing kernel size (Section 2.3.3.1), (2) early perimeter adjustment (Section 2.3.3.2), (3) parallax terrain correction (Section 2.3.3.3), and (4) confidence threshold optimization (Section 2.3.3.3) (Figure 3). For GOFER-East and GOFER-West, we separately optimize the confidence threshold and parallax adjustment factor and calculate the smoothing kernel size and early perimeter adjustment. Software details specific to GEE are provided in Appendix B.1.

2.3.3.1 Dynamic kernel size

As described above, the radius of the square kernel used for smoothing is calculated as the spatial resolution of the combined GOES grid within the AOI polygon. Opting for a dynamic kernel size, instead of a static value of 2 km used in Restif and

https://doi.org/10.5194/essd-2023-389
Preprint. Discussion started: 27 September 2023

Hoffman (2020) for example, allows the algorithm to be applied more effectively to fires outside California. The GOES spatial resolution per pixel decreases away from the equator and toward the edge of the disk (Figure B1). The kernel size is calculated in the pre-processing stage and added to the input metadata dictionary.

2.3.3.2 Early perimeter adjustment

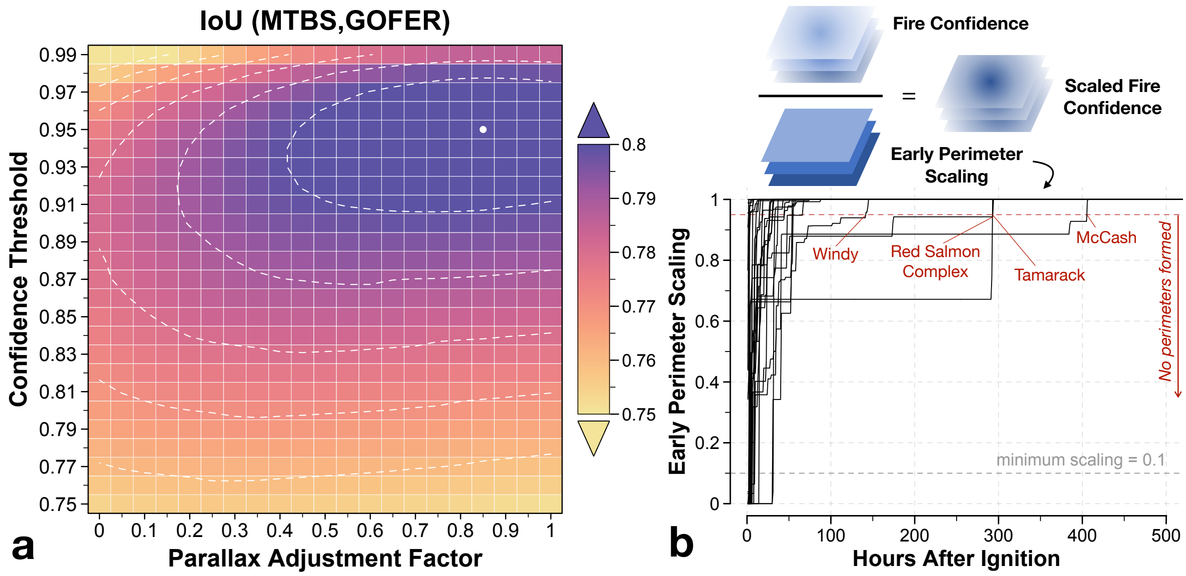

Figure 4: Parameter optimization and early perimeter adjustments for deriving the GOFER-Combined fire progression perimeters. (a) Parameter optimization of the confidence threshold and parallax adjustment factor. The optimization is based on the IoU of GOFER and MTBS perimeters at the final extent of the fire, averaged across the 10 largest CA fires in 2020. At the maximum IoU, the optimized confidence threshold is 0.95, and the parallax adjustment factor is 0.85. (**b**) **Early perimeter scaling**. Adjustment for the fire confidence of early perimeters is shown as a function of hours after ignition, with individual lines depicting each of the 28 largest fires in CA from 2019-2021. The hourly fire confidence is divided by the early perimeter scaling to calculate the scaled fire confidence. The minimum scaling, denoted by the dashed gray line, is set at 0.1 to prevent overly inflating early perimeters. The optimized confidence threshold of 0.95 for GOFER-Combined is denoted by the dashed red line. When the early perimeter scaling is lower than the confidence threshold, a perimeter cannot be formed without any adjustment. The four fires depicted would have had their first perimeter formed hundreds of hours after ignition without the early perimeter scaling.

Some fires smolder at low intensity, leading to low confidence detections at the beginning of their lifetime. Consequently, the GOFER algorithm fails to output these early perimeters as the confidence values do not meet the required threshold. We add an adjustment to “anchor” the first perimeter at or close to the first available GOES fire detection by scaling the fire detection confidence. For each hour, the scaling factor is calculated as that hour’s confidence divided by the maximum of the cumulative maximum confidence up to that hour. The scaling factor ranges from 0 to 1, where 1 indicates no scaling; however, we set the minimum scaling factor to 0.1 to prevent overinflation of early perimeters (Figure 4b). To perform the early perimeter adjustment, the hourly maximum confidence is divided by the scaling factor.

2.3.3.3 Confidence threshold optimization and parallax correction

Next, we simultaneously optimize for the confidence threshold and parallax adjustment factor. The confidence threshold applies a mask to the smoothed fire detection confidence and removes values lower than the threshold. The parallax adjustment factor

https://doi.org/10.5194/essd-2023-389
Preprint. Discussion started: 27 September 2023

ranges from 0-1 and is multiplied by the parallax displacement in the x and y-components; this range allows us to test the efficacy of the parallax correction on the spatial accuracy of the final perimeter. The parallax correction algorithm is a function of the terrain elevation, the height of the satellite, the longitudinal position of the satellite, Earth's semi-minor and semi-major axis, and GRS-80 eccentricity (Spestana et al., 2022). We use the USGS 10-m 3DEP DEM as input. The displacement is smoothed using the same square kernel for smoothing the GOES fire detection confidence. This prevents extreme displacements of smaller 10-m pixels within a coarse GOES pixel that may contain large variations in elevation.

For optimization, we test the confidence threshold in increments of 0.01 from 0.75 to 0.99 and the parallax adjustment factor in increments of 0.05 from 0 to 1 (Figure 4a). For each combination of the tested confidence threshold and parallax adjustment factor, we calculate the IoU of the GOFER and MTBS final perimeters. The IoU, or Jaccard index, is a common metric for evaluating spatial accuracy against ground truth data. We take the optimal values at the maximum IoU (Table B2). As this process is computationally intensive, the parameter search uses the 10 largest fires in California in 2020.

2.3.4 Post-processing: Quality control

In the post-processing stage, we undertake quality control of the hourly perimeters. For each timestep, we ensure that the perimeter is spatially inclusive of previous perimeters by taking the union of that perimeter and previous perimeters. We set the last timestep as when the perimeter last grew and remove extraneous perimeters.

https://doi.org/10.5194/essd-2023-389
Preprint. Discussion started: 27 September 2023

Open Access Earth System Science Data Discussions

2.4 Derived fire metrics

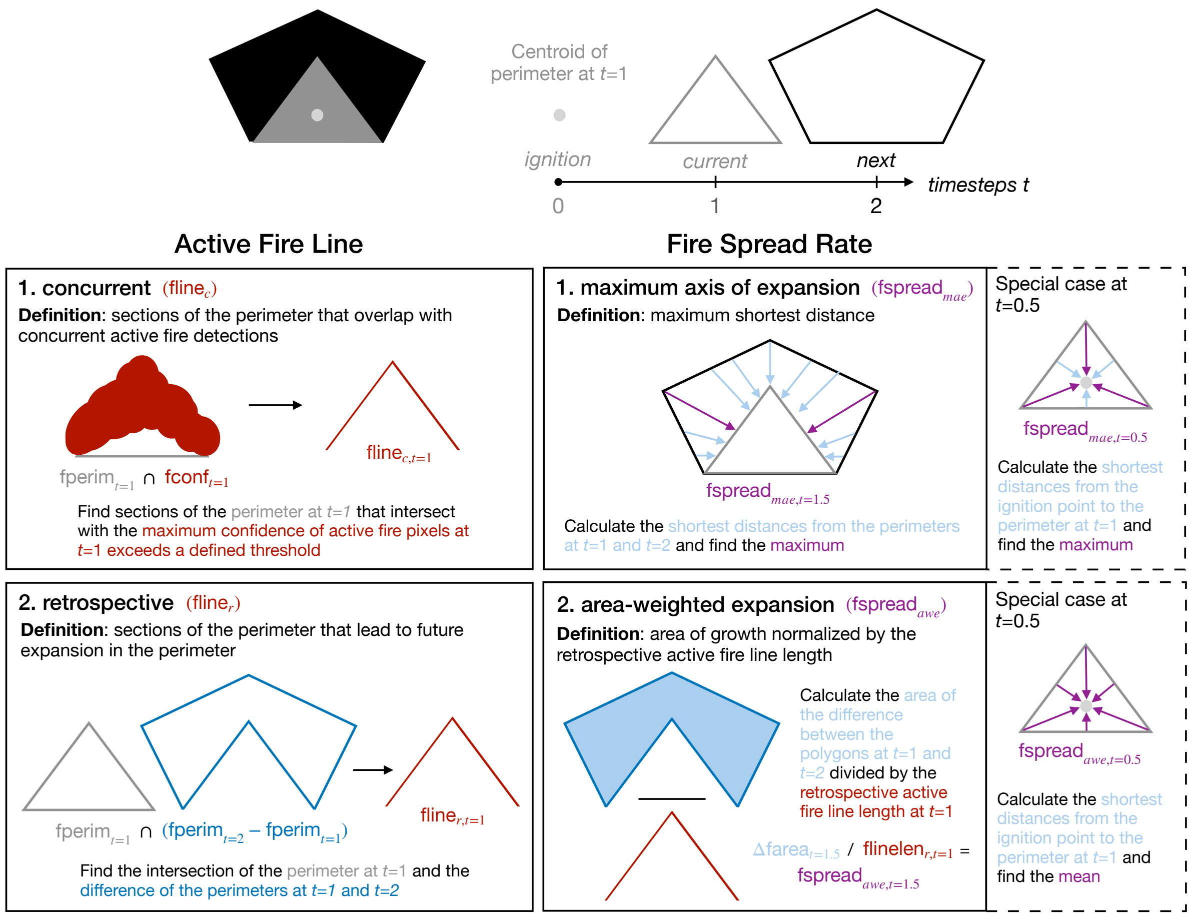

Figure 5: Pictorial overview of definitions for delineating active fire lines and calculating the fire spread rates. A simplified representation of perimeters is shown with the ignition point at timestep t=0, the current perimeter at timestep t=1, and the next perimeter at timestep t=2. We use a 1) concurrent and 2) retrospective method for delineating active fire lines. The "concurrent" method relies on the intersection between the fire perimeter and concurrent active fire detections, while the retrospective method uses future perimeters to determine which portion of the current perimeter leads to a growth in area. We also define the fire spread rate from the 1) maximum axis of expansion (MAE) and 2) area-weighted expansion (AWE). The MAE fire spread rate is calculated from the maximum shortest distance between two perimeters, while the AWE fire spread rate is calculated as the area of growth normalized by the retrospective active fire line length.

From the GOES-derived progression perimeters, we compute several key fire metrics, including the diurnal cycle of the fire growth in units of area (km^2), active fire line length (km), and fire spread rate (km/h). Figure 5 illustrates the methods for calculating the active fire line and fire spread rate. We use simple polygons to depict hypothetical perimeters at timesteps t = 0 to t = 2, or from ignition (t = 0) to the current hour (t = 1) to the next hour (t = 2). The ignition point is defined as the centroid of the perimeter at t = 1.

2.4.1 Active fire line

We identify the active fire line in two ways, as either the "concurrent" or the "retrospective" active fire line. Both active fire line lengths are in units of km.

The concurrent active fire line ($fline_c$) is defined as the segments of a given fire perimeter that intersect with active fire detections of that hour above a certain threshold. We output $fline_c$ at hourly confidence thresholds c of 0.05, 0.1, 0.25, 0.5, 0.75, and 0.9; this set of varying thresholds allows us to progressively narrow down perimeter segments with the most intense burning. A lax threshold, such $fline_{c=0.05}$, uses most of the active fire detections during that hour, while a strict threshold, such as $fline_{c=0.9}$, only uses high confidence detections to create the hourly GOES fire perimeters. $fline_c$ with stricter thresholds correspond to areas with higher fire intensity. We convert the perimeters from polygons to linestrings and use a buffer of 100 m around the perimeter to extract intersecting active fire pixels with fire detection confidence above the defined threshold.

The retrospective active fire line ($fline_r$) is defined as the segments of a given fire perimeter that leads to growth in the next hour's perimeter. Because of this strict definition, the $fline_r$ is generally shorter than the $fline_c$ that is defined using low confidence thresholds (e.g., c = 0.05), as the latter may include segments of the perimeter that may be actively burning but have not yet expanded during that hour.

For both the $fline_c$ and $fline_r$, we consider the perimeter as "growing" in a given time step if the active fire line length is > 0 and "dormant" otherwise. We fill in "dormant" timesteps with the most recent $fline_c$ prior to that timestep and the most immediate $fline_r$ after that timestep.

$fline_c$ can be calculated in near-real-time along with perimeters and is most useful for identifying potential areas of spread and predicting future perimeters. In contrast, $fline_r$ requires knowledge of future perimeters but offers a more precise estimate of where the perimeter expanded. Thus, $fline_r$ is more useful for studying the trends and behaviors of historical fires.

2.4.2 Fire spread rate

We define the fire spread rate, in units of km/h, in two ways, as either the maximum axis of expansion (MAE) or the area-weighted expansion (AWE) between two hourly timesteps. While the fire perimeter and active fire line describe the state of the fire at the end of the hour (t = 1,2,3…), the fire spread rate, along with the growth in the area, describes the change in state between consecutive perimeters; we thus set these latter variables at the half hour (t = 0.5,1.5,2.5…). For example, the fire spread rate at t = 1.5 is calculated from the perimeters at t = 1 and t = 2.

The MAE fire spread rate ($fspread_{MAE}$) is calculated as the maximum shortest distance between consecutive perimeters. For the $fspread_{MAE}$ at t = 1.5, we calculate the shortest distance from the perimeter at t = 1 outward to all pixels within a search radius of 100 km. We then extract the maximum distance value within the area of growth between the perimeters at t = 1 and t = 2. In the case where there is no previous perimeter, such as the $fspread_{MAE}$ at t = 0.5, we set the previous perimeter, at t = 0, as the centroid of the perimeter at t = 1. In the case of fires merged from smaller fires, we disaggregate multipolygons into separate polygons and search for new ignitions or polygons that do not overlap with the previous perimeter. If no overlap exists for a polygon, we add the centroid of that polygon to the previous perimeter.

The AWE fire spread rate ($fspread_{AWE}$) is calculated as the fire-wide growth in area divided by the retrospective active fire line length. The $fspread_{AWE}$ at t = 1.5, for example, is calculated as the change in area, in km^2, from the perimeter at t = 1 to the perimeter at t = 2 divided by the $fline_r$ length at t = 1. The calculation of $fspread_{AWE}$ for the special case of when there is no $fline_r$ at ignition, or during the timestep just prior to the first formed perimeter (here depicted as t = 0), is similar to that for $fspread_{MAE}$, except here we take the average rather than the maximum.

https://doi.org/10.5194/essd-2023-389
Preprint. Discussion started: 27 September 2023

2.5 GOFER dataset structure and variables

Table 2: Variables in the GOFER dataset.

Name	Short Name	Units
Global variables		
Fire name	fname	
Fire year	fyear	
End-of-hour variables (*t*=1,2,3…)		
Hours after ignition, end of hour	timestep	hours
UTC time	tUTC	
Local time, with daylight savings	tLocal	
Local time, without daylight savings	tLocalGMT	
Area within fire perimeter	farea	km^2
Area within fire perimeter, as a percentage of the final area	fareaPer	%
Active fire line length (concurrent)	cflinelen	km
Active fire line length (retrospective)	rflinelen	km
Length of the perimeter	fperim	km
State of the fire	fstate	0 = dormant, 1 = active
Half-hour variables (*t*=0.5,1.5,2.5…)		
Hours after ignition, half hour	timestep_hh	hours
Growth in fire-wide area	dfarea	km^2
Fire spread rate (MAE)	maefspread	km/h
Fire spread rate (AWE)	awefspread	km/h

The GOFER dataset for the 28 large CA fires contains hourly fire perimeters, active fire lines, and fire spread rates for three GOFER versions: GOFER-Combined, GOFER-West, and GOFER-East (Liu et al., 2023). Table 2 describes variables contained in the GOFER dataset. We provide shapefiles (.shp) of the perimeters and concurrent and retrospective active fire lines and a summary table (.csv) of all end-of-hour and half-hour variables. End-of-hour variables record the state of the fire each hour, while half-hour variables record the change in the fire between two consecutive hours.

2.6 Evaluation and validation

To validate the spatial accuracy of the GOFER perimeters, we calculate the IoU of GOES and FRAP final perimeters. We compare this to the IoU of the FEDS and FRAP final perimeters. We use the fire structure status dataset from CAL FIRE as another way to validate the GOFER perimeters by calculating the number of affected and destroyed structures contained by the final perimeter. Specifically, this evaluates omission error, since damaged and destroyed structures should be located within the final perimeter. Additionally, we track the IoU of GOFER and FEDS perimeters, as well as the fraction of false positives and false negatives, at 12-hourly intervals to check when the GOFER perimeters stabilize in spatial accuracy.

https://doi.org/10.5194/essd-2023-389
Preprint. Discussion started: 27 September 2023

We evaluate the GOFER concurrent active fire lines at the different confidence cutoffs (0.05,0.1,0.25,0.5,0.75,0.9) compared to the FEDS active fire lines. We determine which cutoff leads to the highest agreement with the FEDS active fire lines. However, the GOFER and FEDS algorithms still inherently differ. FEDS can take advantage of the higher spatial resolution of 375-m VIIRS detections to nearly pinpoint the exact fire locations, while using the raw GOES active fire detections can lead to large biases due to the much coarser GOES spatial resolution. Thus, the different GOES confidence cutoffs provide a range of concurrent active fire lengths loosely tied to varying levels fire intensity at the fire front. As another check, we calculate the aggregate 12-h retrospective active fire line lengths for both GOFER and FEDS perimeters.

https://doi.org/10.5194/essd-2023-389
Preprint. Discussion started: 27 September 2023

3 Results and Discussion

3.1 Evaluating the accuracy of the GOFER fire progression perimeters

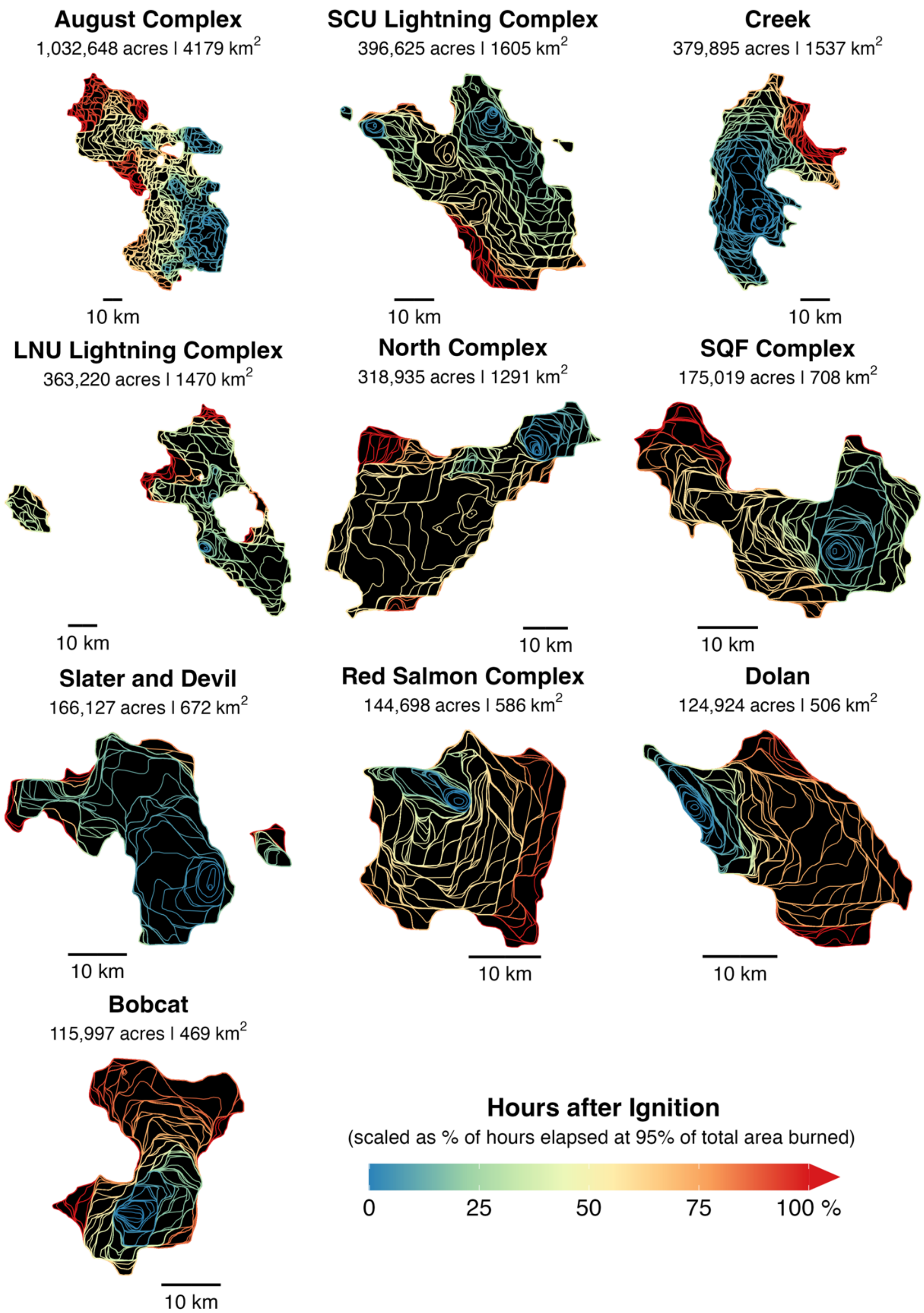

305 **Figure 6: Maps of the GOFER-Combined hourly fire progression perimeters of the 10 large fires over 100,000 acres in CA in 2020.** For each fire, the official burned area in acres and km^2 from CalFire is inset. Cooler colors represent timesteps early

https://doi.org/10.5194/essd-2023-389
Preprint. Discussion started: 27 September 2023

in the fire's lifetime, while warmer colors represent timesteps later in the fire's lifetime. The timesteps are normalized across fires and expressed as the % of hours elapsed relative to the timestep at 95% of total area burned.

Figure 6 shows the hourly GOFER-Combined perimeters for the 10 largest CA fires in 2020 that were used to optimize the confidence threshold and parallax adjustment factor (Figure 4). The optimized confidence threshold is 0.95 for GOFER-Combined, higher than GOFER-East (0.76) and GOFER-West (0.83). The optimized parallax adjustment factor ranges from 0.8 to 1 among the GOFER versions, suggesting that the parallax correction is a needed step to improve the spatial accuracy of GOES active fire pixels (Table B2). Specifically for GOFER-Combined, the mean IoU for the 10 fires is 0.78 when no parallax adjustment is applied (adjustment factor = 0), compared to 0.81 at the optimized adjustment factor of 0.85 (Figure 4a). The effect of the parallax correction is apparent in the Creek Fire, which was located on mountainous terrain at a mean elevation of about 1.8 km above sea level. Its uncorrected final perimeter deviates from the FRAP perimeter on the northern and eastern edges, lowering the IoU by 0.09. (Figure B3).

We evaluate the spatial accuracy of GOFER fire perimeters at the final timestep compared to FRAP and in 12-h intervals compared to FEDS. For the 28 large fires, the mean IoU of GOFER and FRAP perimeters is 0.77 for GOFER-Combined, 0.67 for GOFER-East, and 0.75 for GOFER-West (Table C1). In general, the lower IoU for GOFER-East, due to the coarser resolution of GOES-East compared to GOES-West in California, suggests that GOES-West drives the improved spatial accuracy of the GOFER-Combined perimeters. Because of the larger smoothing kernels used in GOFER-East, the perimeters generally smooth over burned peninsula and inlet-type features where the fire conforms to the sinuous, mountainous terrain (Figure C1, Tables B2, C2).

https://doi.org/10.5194/essd-2023-389
Preprint. Discussion started: 27 September 2023

Open Access Earth System Science Data Discussions

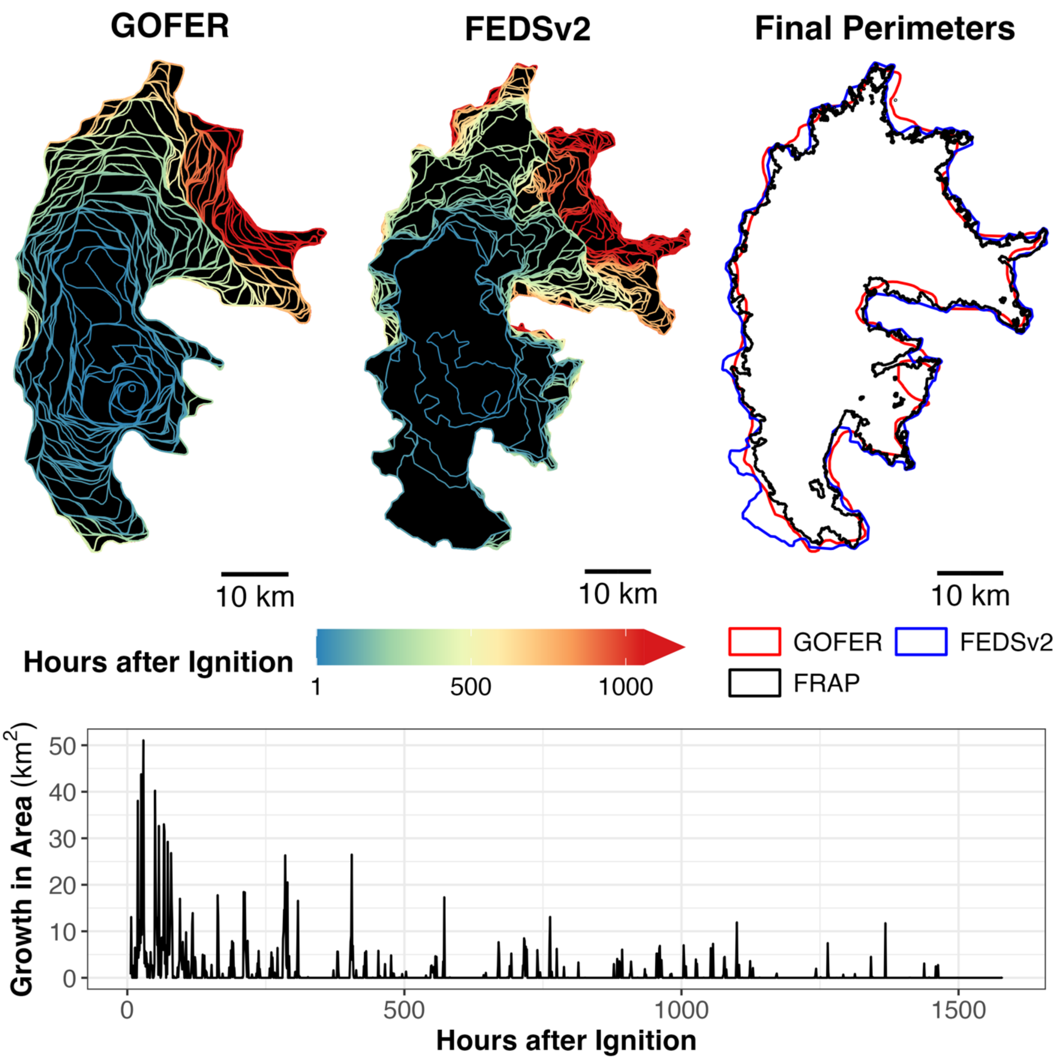

330 **Figure 7: Spatio-temporal progression and comparison of the 2020 Creek Fire.** (*Top panels*) Maps of the hourly GOES-derived GOFER-Combined progression (*left*), 12-hourly VIIRS-derived FEDSv2 progression (*middle*), and comparison of the GOFER-Combined, FEDSv2, and FRAP final perimeters of the Creek Fire (*right*). (*Bottom panel*) Timeseries of the hourly growth in area for the Creek Fire from GOFER-Combined.

Figure 7 compares the Creek Fire progression mapped by GOFER-Combined and FEDSv2. Although the FEDS perimeters are more detailed, GOFER fills in gaps in the fire progression when the fire spreads rapidly (< 50 h after ignition for the Creek Fire), thereby providing insights into the fire's behavior when it is most explosive. We also compare the IoU of GOFER to FEDS relative to FRAP for 25 large fires, which excludes the three cross-border fire that are not fully mapped in FEDSv2 (Section 2.1).

https://doi.org/10.5194/essd-2023-389
Preprint. Discussion started: 27 September 2023

Open Access Earth System Science Data Discussions

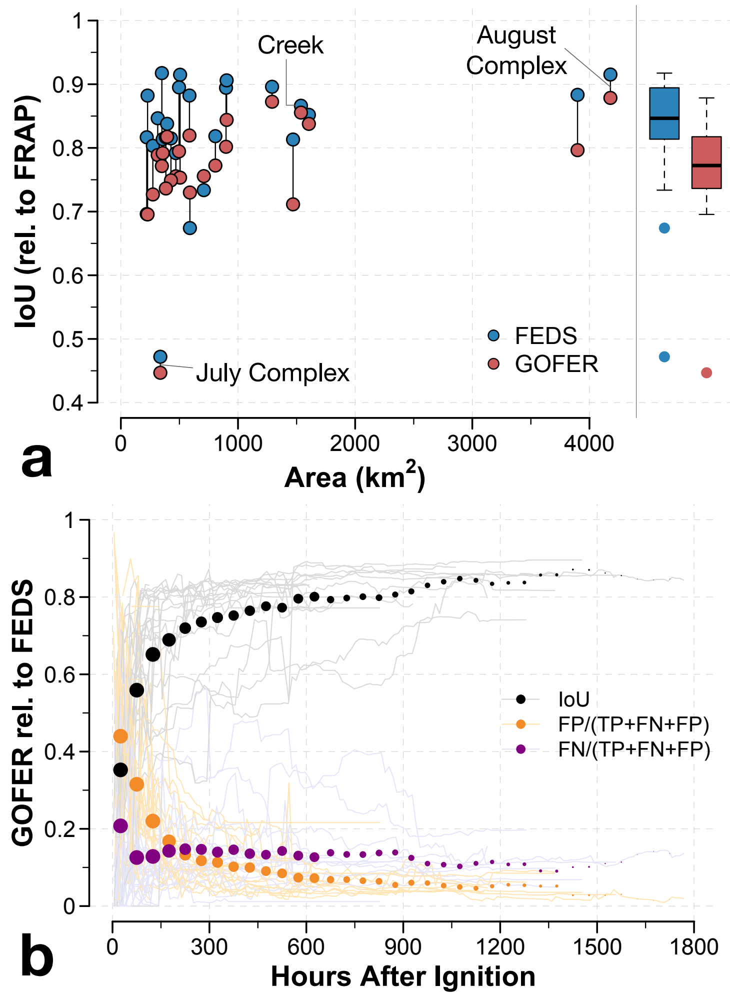

Figure 8: Spatial accuracy of GOFER perimeters compared to FRAP and FEDS. (a) IoU of GOFER and FEDS final perimeters compared to FRAP for large fires in 2019-2021. The vertical lines connect GOFER and FEDS IoU for the same fires.
340 **(b)** Accuracy metrics for evaluating GOFER against FEDS perimeters at 12-h intervals for large fires in 2019-2021. Along with the IoU, we show the fraction of false positives (FP) and false negatives (FN) within the union of the GOFER and FEDS perimeters (TP+FN+FP). In equivalent terms, IoU is the fraction of true positives (TP) within the union. Lines show the accuracy metrics for individual fires, while dots show the average of all fires in 50-h bins. The size of the dots represents the number of fires in each 50-h bin. Fires that straddle the border between CA and a neighbor state (i.e., Slater and Devil, Tamarack, W-5 Cold
345 Springs) were excluded since FEDS perimeters cut off at the CA border.

The IoU for FEDS is 0.83, higher than the IoU of 0.77 for GOFER-Combined, 0.68 for GOFER-East, and 0.76 for GOFER-West (Figure 8a, Table C1). This discrepancy is reasonable considering the higher spatial resolution of the input active fires in FEDS (375 m) compared to GOFER (GOES-East: 3.1-3.6 km, GOES-West: 2.5-2.6 km, Combined: 1.6-1.7 km). In addition, the
350 average IoU of the 10 megafires in 2020 used to optimize parameters is similar to 7 megafires in 2021 (e.g., the IoU for GOFER-Combined and FRAP is 0.8 for 2020 fires and 0.78 for 2021 fires). The lack of a significant drop in IoU suggests that our parameters are not over-tuned to those 10 fires in 2020.

https://doi.org/10.5194/essd-2023-389
Preprint. Discussion started: 27 September 2023

Using FEDS perimeters as 12-h references, we find that the IoU of GOFER and FEDS begins to stabilize around 100 h after ignition (IoU > 0.6) (Figure 8b). At < 100 h, the fires are small and therefore harder to map accurately at GOES resolution, as any small shift in the perimeter can lead to a sizeable decrease in IoU. Another reason for the low IoU < 100 h after ignition is that some fires required extensive early perimeter adjustment to scale the fire detection confidence and output a rough estimate of these early perimeters. In particular, the fraction of false positives is higher than that of false negatives close to ignition due to overinflation in GOFER early perimeters. At the cost of spatial accuracy, we anchor the first perimeter close or at the timestep with the first GOES active fire detection. If the scaling factor from the early perimeter adjustment is lower than the confidence threshold, this indicates that a perimeter could not be formed. In extreme cases, such as the Windy, Tamarack, Red Salmon Complex, and McCash fires for GOFER-Combined, we see this inability to form an initial perimeter hundreds of hours after ignition (Figure 4b).

Certain conditions or features lower the spatial accuracy or IoU – namely, the obscuration of the satellite view due to clouds and heavy smoke, location of a fire along a coastal boundary or water bodies, and presence of unburned islands and narrow burn scar features. Of the 28 fires, the main outlier is the July Complex Fire, which has a low IoU of 0.45 for GOFER-Combined and 0.47 for FEDS (Table C1). Because active fire detection relies on discovering instantaneous thermal anomalies, clouds or thick smoke could prevent both satellite sensors from detecting active fires. On the other hand, burned area mapping, such as in MTBS or FRAP, incorporates a timeseries of pre-fire to post-fire land cover changes, so is possible to infer burned area during very cloudy or smoky periods from later observations. In addition, GOFER tends to underestimate the perimeter extent for fires that hug the coast (e.g., Dolan) or have narrow burn scar features (e.g., LNU Lightning Complex) (Figures 1,6). The neighborhood smoothing in GOFER yields low fire detection confidence values along the edge of the coast and around narrow burn scars, which shrinks the perimeter and can even lead to fragmentation (e.g., SCU Lightning Complex). This issue is more acute in GOFER-Combined, which uses a higher, and therefore stricter, confidence threshold than GOFER-East and GOFER-West. As such, we observe a lower percentage of damaged and destroyed structures within GOFER-Combined (97%) perimeters compared to GOFER-East and GOFER-West (98-100%), signifying higher omission error in GOFER-Combined (Table C3).

3.2 The fire diurnal cycle derived from GOFER

The fire diurnal cycle is commonly derived from the FRP associated with active fires (Andela et al., 2015; Giglio, 2007; Li et al., 2022; Mu et al., 2011; Wiggins et al., 2020). Here we instead track the fire diurnal cycle as the growth in fire-wide area, which the GOFER algorithm makes possible by resolving fire expansion at hourly intervals. Traditionally, burned area products, available at daily to monthly timescales due to algorithm constraints, have lower temporal precision and frequency than needed to resolve diurnal variation (Giglio et al., 2018). As the fire front progresses, we expect the diurnal cycle of the fire-wide growth in area to coincide with or even precede that of active fires and FRP. This is because of lingering fuel load behind the fire front that takes more time to fully burn through, resulting in active fire detections inside the fire perimeter. Maxima in the diurnal cycle occur when the weather is hot, dry, and windy, such as in the afternoon, allowing the fire to easily burn through nearby dry fuels. Minima tend to occur when the weather is cool, wet, and stagnant, such as at night, when nearby fuels are too moist to catch on fire, thereby preventing fire spread (Balch et al., 2022).

https://doi.org/10.5194/essd-2023-389
Preprint. Discussion started: 27 September 2023

Open Access Earth System Science Data Discussions

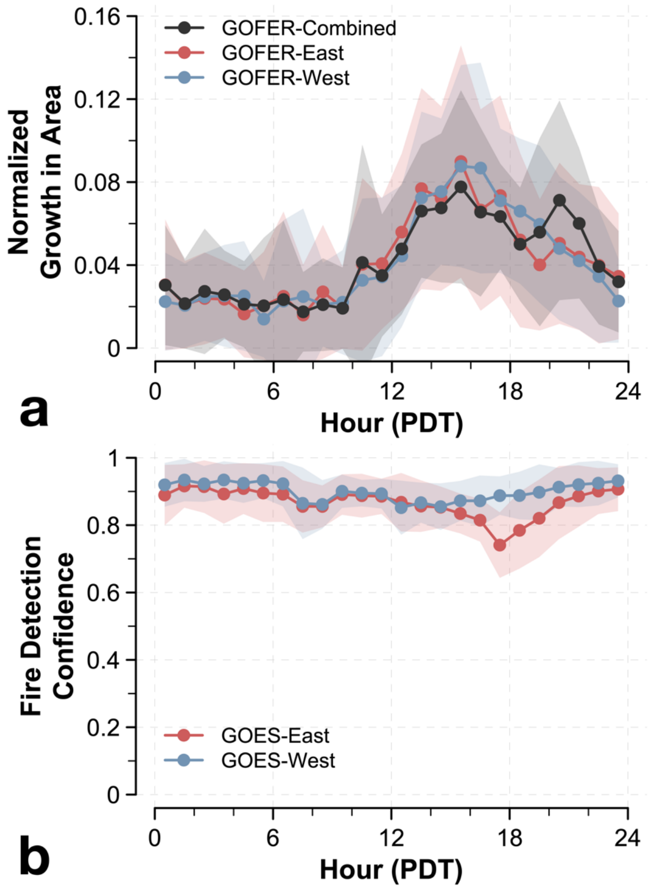

Figure 9: Average GOFER-derived fire diurnal cycle for 28 large CA wildfires from 2019-2021. The diurnal cycle is shown as the normalized hourly fraction of the (**a**) growth in area derived from the GOFER progression perimeters and (**b**) GOES fire detection confidence. For (**b**), the spatial average is calculated from the maximum fire detection confidence of each pixel for each hour.

We derive the fire diurnal cycle from the hourly fire-wide growth in area of the GOFER perimeters. For GOFER-Combined, we observe two peaks in fire perimeter expansion during the afternoon (2-3 pm PDT) and evening (7-8 pm PDT), while GOFER-East and GOFER-West yield a single peak in growth during the afternoon (2-4 pm PDT) (Figure 9a). The diurnal cycle of fire growth in GOFER-Combined closely mirrors that of GOES FRP (Wiggins et al., 2020). During afternoon to evening hours (1-10 pm PDT), GOES-East, when compared to GOES-West, has higher peak-to-valley differences in FRP (-66% vs. -27%) and fire detection confidence (-18% vs. -8%), with noticeable minimums occurring during the day-to-night transition period (4-8 pm PDT) (Figure 9b); similarly, the GOES-East active fire pixel count deviates from that of GOES-West by -7% on average during the same hours. Because GOES-East observes California toward the edge of its disk view (Figure B1), high solar zenith angles, sun glint issues, and mountainous terrain may explain the missed fire detections and lower fire detection confidence (Li et al., 2022). There may also be a positive nighttime fire detection bias as smaller, cooler thermal anomalies are more easily distinguishable relative to the cooler background. Since the GOES-East and GOES-West fire detection confidence are averaged, missed GOES-East detections can lead to false negatives, or burned area that is excluded from the perimeter. An example of this issue is seen on the southeastern edge of the Creek Fire, where the lack of GOES-East active fires led to an unburned inlet carved into the GOFER-Combined perimeter (Figure C1).

https://doi.org/10.5194/essd-2023-389
Preprint. Discussion started: 27 September 2023

The lower reliability of GOES-East during the day-to-night transition period likely drives the temporal artifacts in the fire diurnal cycle in GOFER-Combined. Since GOFER-Combined uses a higher confidence threshold, the algorithm is more sensitive to missed or low-confidence detections, and the fire growth in those late afternoon hours will then be misallocated to evening hours. Even though GOFER-East relies only on GOES-East observations, its optimized confidence threshold (0.76) is less stringent than GOFER-Combined (0.95). Low-confidence active pixels are less likely to be rejected in forming the hourly perimeter, thus resulting in more realistic diurnal cycles of fire growth in GOFER-East and GOFER-West compared to GOFER-Combined. This is a main limitation and area of future work for the GOFER-Combined algorithm, as corrections are needed to boost the fire detection confidence during the day-to-night transition and assign different weights to GOES-East and GOES-West observations.

3.3 Assessing the GOFER active fire lines and fire spread rates

Unlike $fline_r$, the $fline_c$ does not necessarily lead to perimeter expansion (e.g., indicates smoldering or natural/human barriers), but can be used as a near-real-time predictor of fire growth. The $fline_r$ is a stricter definition of the active fire line, more similar in length to $fline_c$ at high confidence thresholds. The $fline_r$ can be used for retrospective analysis to assess the drivers and barriers of fire growth. For GOFER-Combined, the maximum $fline_{c=0.05}$ lengths range from 40 to 264 km, while $fline_r$ lengths range from 19 to 114 km (Table 1).

https://doi.org/10.5194/essd-2023-389
Preprint. Discussion started: 27 September 2023

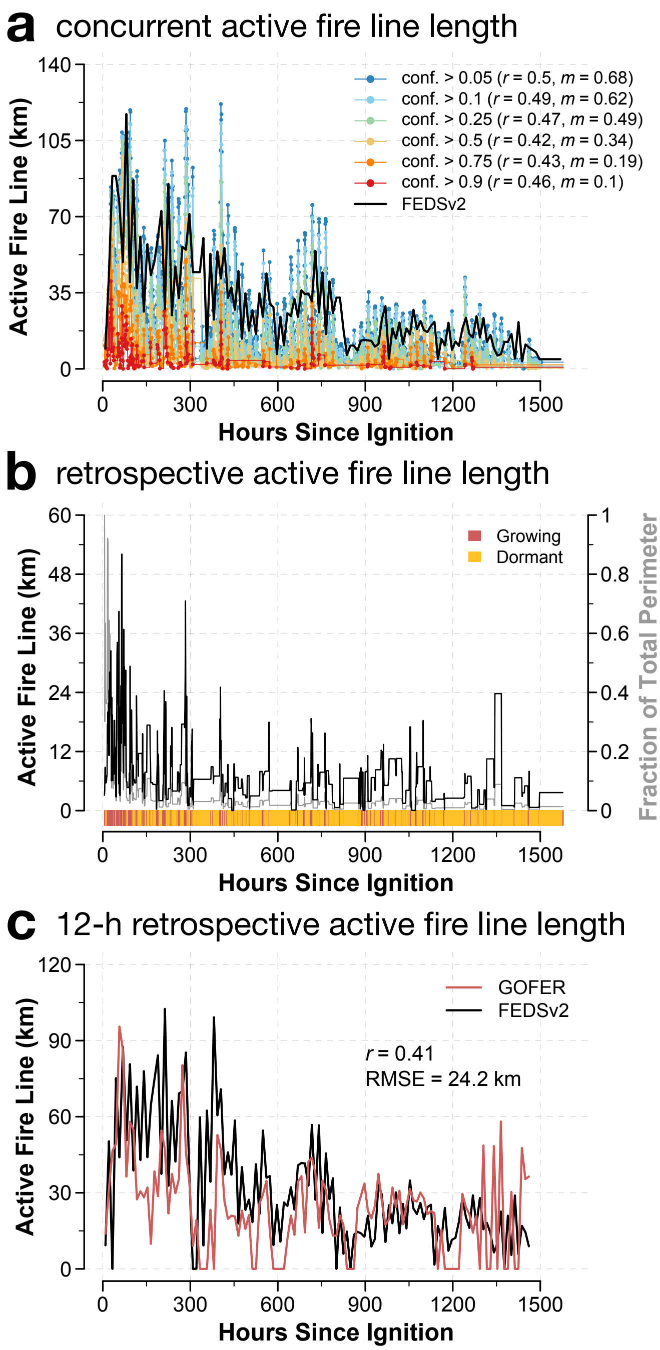

Figure 10: A comparison of GOFER-Combined and FEDS concurrent and retrospective active fire line lengths for the 2020 Creek Fire. (a) Concurrent active fire lengths derived from GOFER perimeters and concurrent active fire detections are
425 shown in colored lines for different fire detection confidence cutoffs (0.05, 0.1, 0.25, 0.75, and 0.9). The 12-h FEDSv2 active fire line lengths are depicted by the black line. The correlation coefficient (r) and slope (m) between GOFER and FEDSv2 active fire line lengths are shown in the inset. **(b)** Retrospective active fire line lengths derived from GOFER perimeters are depicted by the black line. The fraction of the active fire line length with respect to the total perimeter length is depicted by the gray line. The bottom bar shows when the perimeter is growing (red) or dormant (orange). **(c)** 12-h aggregate retrospective active fire line
430 lengths derived from GOFER (red line) and FEDSv2 (black line) perimeters. All correlations shown are statistically significant at $p < 0.05$.

https://doi.org/10.5194/essd-2023-389
Preprint. Discussion started: 27 September 2023

Figure 10 shows the timeseries of the GOFER-Combined $fline_c$ and $fline_r$ active fire lengths and FEDSv2 active fire lengths for the Creek Fire. Both $fline_c$ and $fline_r$ lengths peak soon after ignition and gradually decrease as the fire expansion slows down (Figure 10a-b). Based on the correlation coefficient and slope, the FEDSv2 active fire line lengths are the closest to $fline_{c=0.05}$ (r = 0.5, m = 0.68, p < 0.05) at 12-h intervals (Figure 10a). The calculation of $fline_c$ in the FEDS algorithm is slightly different from the GOFER method as the FEDS input active fire data are represented as points rather than images of the fire detection confidence. To directly compare the two datasets, we use the same method to derive the 12-h aggregate $fline_r$ from FEDS and GOFER perimeters. For the Creek Fire, the $fline_r$ lengths are moderately correlated (r = 0.41, p < 0.05) with a RMSE of 24.2 km (Figure 10c). GOFER tends to underestimate the $fline_r$ length, with more values of 0, suggesting that some areas of expansion are not as well captured. This is partly because GOFER perimeters are less sinuous due to the lower spatial resolution of GOES and the neighborhood smoothing applied in the algorithm (Table C3).

For the 25 large CA fires, excluding cross-border fires, the overall correlation coefficient and slope between $fline_c$ and FEDS active fire line lengths decrease as the confidence threshold increases, while the RMSE increases (Figure C4). As such, the $fline_{c=0.05}$ should be considered as the default $fline_c$, with the $fline_c$ at higher confidence thresholds representing areas with increased likelihood of fire perimeter expansion. Relative to FEDS, GOFER-East $fline_r$ and $fline_c$ have consistently lower accuracy than GOFER-Combined and GOFER-West. For GOFER-Combined, the $fline_{c=0.05}$ has an average r = 0.45 ± 0.26, slope = 0.44 ± 0.25, and RMSE = 21 ± 11 km; the 12-h aggregate $fline_r$ has an average r = 0.64 ± 0.19, slope = 0.59 ± 0.23, and RMSE = 17 ± 10 km (Figure C2).

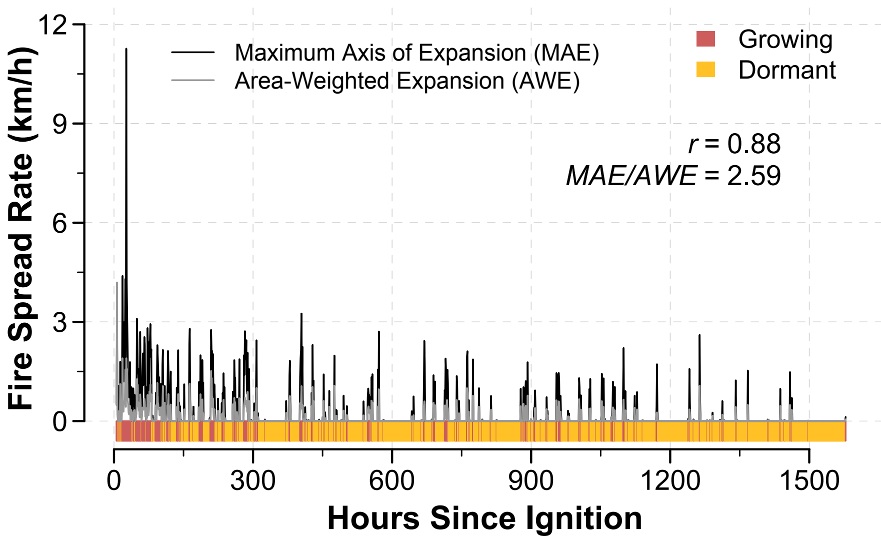

Figure 11: Hourly fire spread rate derived from GOFER-Combined perimeters for the 2020 Creek Fire. The fire spread rate is calculated using two methods: maximum axis of expansion (MAE, black line), and area-weighted expansion (AWE). The correlation coefficient (r) between the MAE and AWE fire spread rates and MAE/AWE ratio are shown inset. The bottom bar shows when the perimeter is growing (red) or dormant (orange).

Figure 11 shows the timeseries of fire spread rates calculated using two different methods ($fspread_{MAE}$, $fspread_{AWE}$) for the Creek Fire. The hourly $fspread_{MAE}$ and $fspread_{AWE}$ are strongly correlated (r = 0.88, p < 0.05), with $fspread_{MAE}$ 2.59 times as high as $fspread_{AWE}$. For all 28 large CA fires, we find strong correlations of r = 0.93 ± 0.05 for GOFER-Combined, of r =

https://doi.org/10.5194/essd-2023-389
Preprint. Discussion started: 27 September 2023

0.94 ± 0.02 for GOFER-East, and of r = 0.95 ± 0.02 for GOFER-West (Table C4). The ratio of $fspread_{MAE}$ to $fspread_{AWE}$ is 2.74 ± 0.12 for GOFER-Combined, 2.48 ± 0.15 for GOFER-East, and 2.56 ± 0.13 for GOFER-West. For GOFER-Combined, the maximum $fspread_{MAE}$ ranges from 2.2 to 11.3 km/h, while $fspread_{AWE}$ range from 0.9 to 10.8 km (Table 1). In rare cases, usually early in the fire's lifetime, we find higher $fspread_{AWE}$ than $fspread_{MAE}$ (e.g., Zogg Fire). This happens when the fire grows explosively from a small perimeter and active fire line in the previous timestep.

3.4 Future work and applications

The GOFER dataset can used to address key scientific questions on fire behavior controls in California. For example, what climate and vegetation conditions cause fires to become explosive or quiescent during daytime or nighttime hours? How effective is active suppression in limiting fire spread and damage to structures, particularly during severe fire seasons when resources are spread thin among large, simultaneously burning fires? Applications include creating new machine learning models of fire spread, evaluating fire models, and assessing public health, ecosystem, and economic impacts. Below we discuss the future development and applications of GOFER.

We foresee several extensions and applications of the GOFER algorithm and dataset. First, the GOFER diurnal cycle of the fire-wide growth in area can be used to downscale the perimeters of select fires in existing fire progression datasets, such as FEDS, to hourly intervals. Further, the GOFER algorithm itself can be adjusted to incorporate MODIS, VIIRS, Landsat, and Sentinel observations. Second, the GOFER algorithm can be adapted for observations from other geostationary satellites, such as Himawari over East Asia, Equatorial Asia, and Australia and Meteosat over Europe and Africa (Hally et al., 2016; Roberts and Wooster, 2008). Third, the GOFER dataset can be used to build temporal or spatio-temporal statistical and machine learning models to understand how variations in climate, suppression, and fuels drive fire spread rate and fire-wide growth in area. GOFER perimeters can be used to validate existing 3D fire spread models or initialize such models using the active fire lines. Additionally, the GOFER dataset can be used to explore periods of critical stress on firefighting resources, such as in mid-August and early September of 2020 when 8-9 large fires were simultaneously active (Figure A1). Fourth, GOFER can be used to improve the fire diurnal cycle for atmospheric modeling of smoke emissions. In current global fire emissions datasets, such as the Global Fire Emissions Database, the fire diurnal cycle is broadly generalized by land cover and generally static from day to day throughout a fire's lifetime (Mu et al., 2011; van der Werf et al., 2017). However, large fires may have explosive days of growth where burning extends from the afternoon to evening, while other days with slower fire spread are generally marked only by growth during the afternoon peak. Understanding this variability in fire activity can better inform air quality forecasts and plume tracking with other satellite observations.

A useful direction for future work would be to apply the GOFER algorithm to a diverse sample of large fires across the GOES domain and test how its performance varies using observations from one or both satellites. Ground truth data for other regions may include perimeters provided by state and federal agencies or high-resolution burned area mapping from Landsat and Sentinel. How GOFER-East and GOFER-West perform relative to each other depends largely on the longitudinal location of a given fire relative to the longitudinal position of the GOES satellites. We show that GOFER-West (IoU = 0.75) outperforms GOFER-East (IoU = 0.67) in mapping California fires, but we can also hypothesize that the reverse is true for fires in the Amazon and other biomes in South America. The spatial accuracy of mapping perimeters is influenced by substantial heterogeneity in the magnitude in parallax displacement and GOES pixel resolution across the GOES domain (Figures B1, B2). We can thus expect higher mapping accuracy for fires located at the center of the disk, near the equator, and/or low elevation than those at the edge of the disk, far from the equator, and/or high elevation.

https://doi.org/10.5194/essd-2023-389
Preprint. Discussion started: 27 September 2023

Open Access Earth System Science Data Discussions

As the GOFER algorithm is applied to fires outside California, small adjustments may include further optimizing tunable parameters. We currently implement a dynamic smoothing kernel size, the optimization for the confidence threshold and parallax adjustment factor, and early perimeter adjustment. First, the smoothing kernel, which applies a neighborhood mean, removes the "blockiness" of the fire perimeter polygon that conforms to the pixelated footprint of the fire confidence raster. Dynamically setting the smoothing kernel size equal to the GOES spatial resolution at a fire's location eliminates this "blockiness" and provides a universal method to calculate the smoothing kernel size for fires across the GOES domain. However, this smoothing induces errors in some fire perimeters that hug the coast, contain unburned islands (e.g., water bodies), or encompass narrow swaths of burned area. To address these limitations, rules can be implemented for how the smoothing kernel is applied, such as according to nearby land cover. Second, we optimize the confidence threshold and parallax adjustment factor based on the IoU of GOFER and MTBS of the 10 largest fires in California in 2020. The two parameters can be tuned per fire, but this may lead to over-tuning and substantially increases computation time. Additional optimization metrics may be considered, such as the maximum distance between true positive and either false positive or false negative pixels, used by Google's current wildfire tracking system based on machine learning methods (Ben-Haim and Nevo, 2023). The kernel size for smoothing the fire detection confidence, and the shape of the kernel itself, can also be tested as an additional tunable parameter. Future development of GOFER should consider how the optimal set of parameters differs by region and land cover by tuning the parameters on subsets of fires. Third, we apply early perimeter adjustment to anchor the first perimeter close to or at the first GOES active fire detection. The early perimeter adjustment works by increasing the fire confidence if the maximum value is between 0.1 and 1. This adjustment targets fires that smolder for a long time before rapidly expanding, where the confidence of the GOES detections does not meet the threshold to create a perimeter. Additionally, since the footprint of a fire early in its lifetime (< 50 h after ignition) often encompasses only one to a few GOES active fire pixels, the spatial accuracy of the GOFER early perimeters is low compared to FEDS (IoU < 0.5). One potential adjustment is shrinking each perimeter by its scaling factor (i.e., if < 1) to prevent overly inflating early perimeters derived from low confidence detections. This process can then be tested on timesteps with a maximum confidence below the minimum threshold of 0.1, which currently yield no perimeters; if successful, this adjustment will anchor the first perimeter of every fire to the timestep with the first GOES active fire detection.

Additional potential development areas include the adjustment of the fire detection confidence and the automation of the GOFER algorithm for use in near-real-time. First, in GOFER, we currently convert the GOES fire mask codes to fire detection confidence following Restif and Hoffman (2020). To improve GOFER's spatial accuracy, we can integrate GOFER with MODIS and VIIRS observations. However, testing is needed to adjust the fire detection confidence calculation with the MODIS and VIIRS active fire products. Although the confidence threshold optimization matches final perimeters in GOFER with MTBS, resulting in spatial accuracy comparable to FEDS, a closer investigation is needed to assess how GOES fire mask codes compare to those in other active fire products. For example, the 375-m VIIRS active fires (VNP14IMGML) are assigned with only three possible detection confidence categories ("low", "medium", and "high"), while the 1-km MODIS active fires (MCD14ML) are assigned a detection confidence that ranges from 0 to 100. Second, the GOFER algorithm is currently semi-automated and processes each fire separately, relying on manual updates to a metadata dictionary containing that fire's bounding box and start and end time. Here we tested the GOFER algorithm on fires over 50,000 acres (202 km^2), but the lower size limit of fires that GOFER can map effectively should be explored. For operational, near-real-time use, GOFER needs to be able to identify individual fire events and determine these constraints automatically.

https://doi.org/10.5194/essd-2023-389
Preprint. Discussion started: 27 September 2023

4 Conclusion

In summary, we use GOES observations to develop the GOFER algorithm for deriving the hourly fire progression perimeters, active fire lines, and fire spread rates of large wildfires. We test the algorithm for 28 fires over 50,000 acres (202 km^2) in California from 2019-2021. We implement a parallax terrain correction with optimizations for the parallax adjustment factor and confidence threshold, early perimeter adjustment, and a dynamic kernel for neighborhood smoothing. Relative to reference perimeters provided by FRAP, the spatial accuracy of GOFER (IoU = 0.77) is reasonable compared to the VIIRS-derived FEDSv2 (IoU = 0.83) at 375-m spatial resolution. We apply two different methods to map active fire lines (concurrent and retrospective) and calculate fire spread rates (MAE and AWE). GOFER resolves the time dimension of fire progression mapping to hourly intervals and provides new insights into critical, explosive periods of fire spread. Opportunities for future development of the GOFER algorithm include resolving the day-to-night transition issues that skew the fire diurnal cycle of the fire-wide growth in area and testing GOFER in different ecosystems and regions across the GOES domain. Additionally, our GOFER dataset for the 28 large wildfires in California from 2019-2021 is a useful reference for modeling climate-human-fire relationships and improving estimates of fire emissions and smoke pollution.

https://doi.org/10.5194/essd-2023-389
Preprint. Discussion started: 27 September 2023

Appendix A: Study Area: Large Wildfires in California

Table A1: Metadata for the 28 large wildfires in California from 2019-2021 over 50,000 acres (202 km^2). Statistics are from the annual CAL FIRE Red Books, which provide detailed information on each fire. The coordinates (longitude, latitude) and ignition times (year-month-day hour) are from CAL FIRE and InciWeb; some ignition times are adjusted earlier if there are preceding GOES active fire detections.

#	**Fire Name**	**Year**	**Area** (acres)	**Area** (km^2)	**Lon**	**Lat**	**Ignition** (UTC)
1	Kincade	2019	77758	315	-122.78	38.79	2019-10-24 04
2	Walker		54608	221	-120.68	40.06	2019-09-04 21
3	August Complex	2020	1032648	4179	-122.67	39.78	2020-08-16 21
4	Bobcat		115997	469	-117.87	34.24	2020-09-06 19
5	Creek		379895	1537	-119.26	37.19	2020-09-05 01
6	CZU Lightning Complex		86509	350	-120.68	40.06	2020-08-16 15
7	Dolan		124924	506	-121.60	36.12	2020-08-18 18
8	Glass		67484	273	-122.50	38.56	2020-09-27 10
9	July Complex		83261	337	-121.48	41.70	2020-07-22 17
10	LNU Lightning Complex		363220	1470	-122.15	38.48	2020-08-17 13
11	North Complex		318935	1291	-120.93	40.09	2020-08-17 16
12	Red Salmon Complex		144698	586	-123.43	41.19	2020-08-19 14
13	SCU Lightning Complex		396625	1605	-121.30	37.44	2020-08-16 11
14	Slater and Devil		166127	672	-123.38	41.77	2020-09-08 13
15	SQF Complex		175019	708	-118.50	36.26	2020-08-19 14
16	W-5 Cold Springs		84817	343	-120.28	41.03	2020-08-18 18
17	Zogg		56338	228	-122.57	40.54	2020-09-27 21
18	Antelope	2021	145632	589	-121.93	41.50	2021-08-01 17
19	Beckwourth Complex		105670	428	-120.37	39.88	2021-07-03 17
20	Caldor		221835	898	-120.54	38.59	2021-08-15 01
21	Dixie		963309	3898	-121.38	39.88	2021-07-14 00
22	KNP Complex		88307	357	-118.81	36.57	2021-09-10 14
23	McCash		94962	384	-123.40	41.56	2021-08-01 02
24	McFarland		122653	496	-123.03	40.35	2021-07-30 01
25	Monument		223124	903	-123.34	40.75	2021-07-31 01
26	River Complex		199359	807	-123.06	41.39	2021-07-30 21
27	Tamarack		68637	278	-119.86	38.63	2021-07-04 18
28	Windy		97528	395	-118.63	36.05	2021-09-10 00

https://doi.org/10.5194/essd-2023-389
Preprint. Discussion started: 27 September 2023

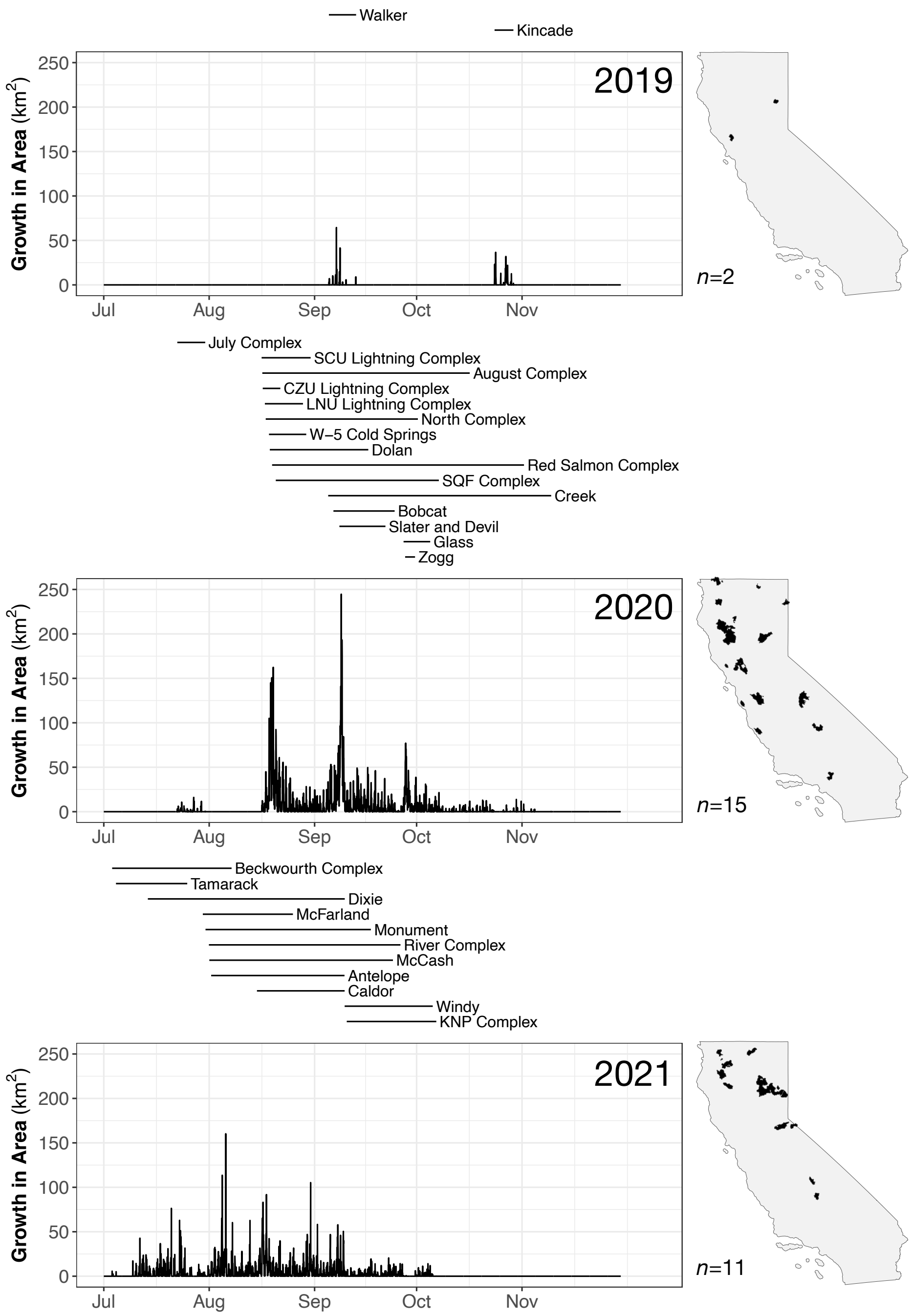

555 **Figure A1: Timeseries of the hourly growth in area from 2019-2021 in the GOFER-Combined dataset.** For each year, the growth in area (km^2) is summed across all fires in each year. The horizontal lines above the timeseries represent the duration of active growth of each fire, ordered by start time. Annual maps of the locations of the fires are shown on the right.

https://doi.org/10.5194/essd-2023-389
Preprint. Discussion started: 27 September 2023

Open Access Earth System Science Data Discussions

Appendix B: Development and Optimizations for GOES-based Mapping of Fire Progression

Table B1: Remapping GOES fire mask categories to continuous fire detection confidence values.

Fire Mask Category		**Fire Detection Confidence**
Description	*Code*	
Processed fire	10	1
Processed fire, filtered	30	
Saturated fire	11	0.9
Saturated fire, filtered	31	
Cloud contaminated fire	12	0.8
Cloud contaminated fire, filtered	32	
High probability fire	13	0.5
High probability fire, filtered	33	
Medium probability fire	14	0.3
Medium probability fire, filtered	34	
Low probability fire	15	0.1
Low probability fire, filtered	35	

B.1 Software details

Input metadata dictionary. For each fire, we set the spatial and temporal constraints for processing GOES active fires by examining the GOES active fire timeseries and spatial footprint. They are necessary to avoid computational timeouts in GEE.

Dynamic kernel. The *reduce neighborhood* function to smooth the fire detection confidence uses the boxcar optimization, which is a fast method for computing the mean but only works with square and rectangular kernels in GEE.

Parallax correction. To implement the GOES parallax correction in Earth Engine, we convert the Python code in the *goes-ortho* package to JavaScript (Spestana et al., 2022). In GEE, we use the *displace* function to correct the location of GOES active fire detections. We separately computed the x- and y-component of the displacement for GOES-East and GOES-West, in meters, between the coordinates (longitude, latitude) of the DEM and satellite perspective as inputs to this function. As a caveat, we must use high-resolution or downscaled DEM, as we find the *displace* function in Earth Engine to be inaccurate if the displacement is less than half the spatial resolution of the DEM.

https://doi.org/10.5194/essd-2023-389
Preprint. Discussion started: 27 September 2023

Table B2: The optimized confidence thresholds and parallax adjustment factors and smoothing kernel sizes used in GOFER.

	Confidence Threshold	Parallax Adjustment Factor	Smoothing Kernel Size
GOFER-Combined	0.95	0.85	1.6-1.7 km
GOFER-East	0.76	0.8	3.1-3.6 km
GOFER-West	0.83	1	2.5-2.6 km

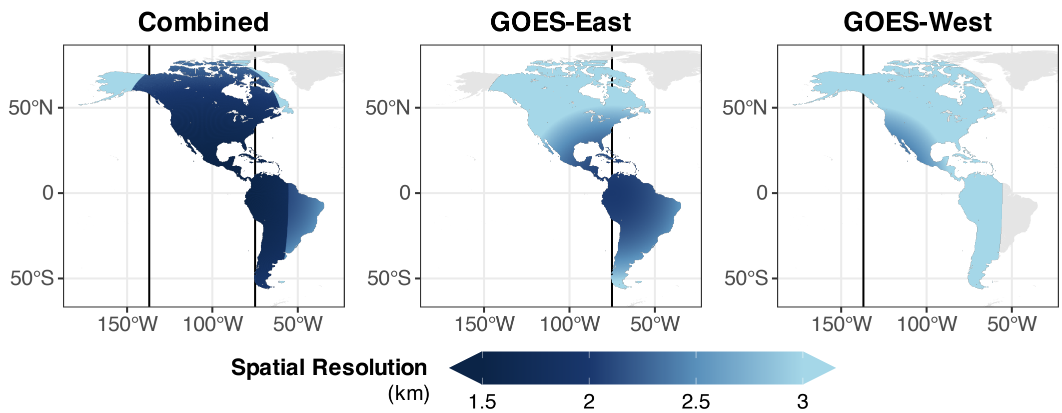

575 **Figure B1: Spatial resolution of GOES-East, GOES-West, and combined GOES across the domain over land.** The GOES spatial resolution, in km, is calculated on the 0.25° x 0.25° grid used by the Global Fire Emission Database, version 4s (GFED4s). Vertical lines depict the longitudinal position of the GOES-East (75°W) and GOES-West (137°W) satellites.

https://doi.org/10.5194/essd-2023-389
Preprint. Discussion started: 27 September 2023

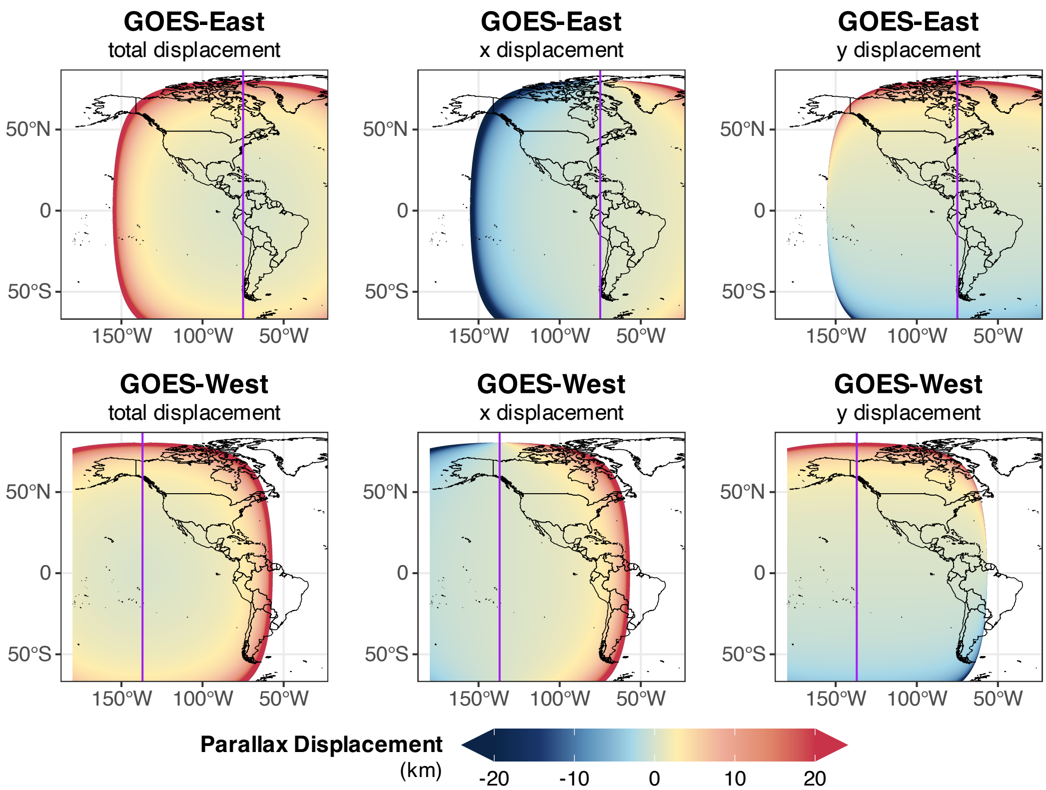

580 **Figure B2: Parallax displacement in GOES-East and GOES-West images across the domain.** The total, x-component, and y-component of the parallax displacement, in km, are calculated for a hypothetical object at 1 km in elevation throughout the domain. For the x-component, negative values indicate that the object is displaced westward, while positive values that the object is displaced eastward. For the y-component, positive values indicate that the object is displaced northward, while negative values indicate that the object is displaced southward. The vertical purple lines depict the longitudinal position of the GOES-East
585 (75°W) and GOES-West (137°W) satellites.

https://doi.org/10.5194/essd-2023-389
Preprint. Discussion started: 27 September 2023

Figure B3: Effect of the parallax terrain correction on the final perimeter, using the Creek Fire as an example. The final perimeter of the Creek Fire with the parallax correction (red polygon) and without parallax correction for GOFER-Combined is shown alongside the FRAP perimeter (black polygon). For the uncorrected perimeter, we use a confidence threshold of 0.91, which yields the highest mean IoU among the 10 largest CA fires in 2020 when the parallax adjustment factor is 0 (Figure 4a).

https://doi.org/10.5194/essd-2023-389
Preprint. Discussion started: 27 September 2023

Table B3: Tunable parameters in the GOFER algorithm.

Tunable Parameter	Definition
Fire mask codes to fire confidence conversion	Definition: converts the codes indicating the quality of active fire detections to numeric values Format: float, [0,1]
Confidence threshold	Definition: delineates the border between burned and unburned area and indicates where to draw the fire perimeter Format: float, [0,1]
Smoothing kernel size	Definition: the radius of the kernel used to apply the neighborhood mean, and smooth the GOES fire confidence Format: float, > 0
Parallax adjustment factor	Definition: the degree to which the parallax terrain adjustment is applied Format: float, [0,1]
Early perimeter scaling	Definition: a scalar used to adjust the maximum fire confidence, relevant for timesteps where the maximum value up to that timestep falls below 1 Format: float, [0,1]

https://doi.org/10.5194/essd-2023-389
Preprint. Discussion started: 27 September 2023

Appendix C: Evaluation and Validation of the GOFER Dataset

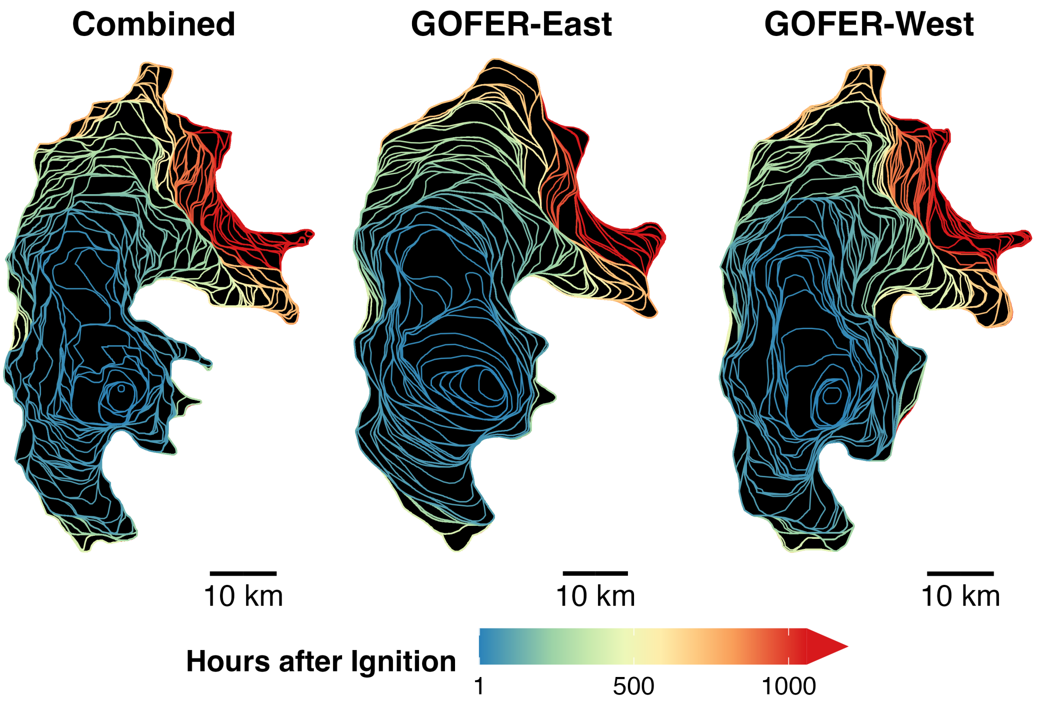

595 **Figure C1: Spatio-temporal progression and comparison of the 2020 Creek Fire.** Maps of the hourly GOFER progression for GOFER-Combined (*left*), GOFER-East (*middle*), and GOFER-West (*right*).

https://doi.org/10.5194/essd-2023-389
Preprint. Discussion started: 27 September 2023

Table C1: IoU calculated for GOFER-Combined, GOFER-East GOFER-West, FEDSv2, and MTBS relative to FRAP.

#	Fire Name	Year	IoU (GOFER, FRAP)			IoU (FEDS, FRAP)	IoU (MTBS, FRAP)
			GOFER-Combined	GOFER-East	GOFER-West		
1	Kincade	2019	0.79	0.72	0.76	0.85	0.99
2	Walker		0.7	0.61	0.71	0.82	0.93
3	August Complex	2020	0.88	0.83	0.87	0.92	0.95
4	Bobcat		0.76	0.63	0.68	0.79	0.98
5	Creek		0.86	0.77	0.83	0.87	0.98
6	CZU Lightning Complex		0.77	0.73	0.87	0.92	0.97
7	Dolan		0.75	0.76	0.74	0.91	0.97
8	Glass		0.73	0.62	0.69	0.8	0.99
9	July Complex		0.45	0.52	0.49	0.47	0.98
10	LNU Lightning Complex		0.71	0.68	0.73	0.81	0.97
11	North Complex		0.87	0.73	0.87	0.9	0.98
12	Red Salmon Complex		0.82	0.73	0.83	0.88	0.97
13	SCU Lightning Complex		0.84	0.79	0.84	0.85	0.97
14	Slater and Devil*		0.77	0.64	0.78	–	0.98
15	SQF Complex		0.76	0.66	0.71	0.73	0.96
16	W-5 Cold Springs*		0.79	0.59	0.74	–	0.98
17	Zogg		0.7	0.56	0.76	0.88	0.99
18	Antelope	2021	0.73	0.6	0.73	0.67	0.95
19	Beckwourth Complex		0.75	0.53	0.71	0.81	0.96
20	Caldor		0.8	0.71	0.8	0.89	0.97
21	Dixie		0.8	0.68	0.78	0.88	0.97
22	KNP Complex		0.79	0.67	0.76	0.81	0.98
23	McCash		0.74	0.65	0.73	0.82	0.97
24	McFarland		0.79	0.75	0.71	0.9	0.97
25	Monument		0.84	0.76	0.84	0.91	0.98
26	River Complex		0.77	0.65	0.74	0.82	0.92
27	Tamarack*		0.69	0.53	0.63	–	0.95
28	Windy		0.82	0.7	0.77	0.84	0.99
Mean IoU (all fires)			0.77 ± 0.08	0.67 ± 0.08	0.75 ± 0.08	–	0.97 ± 0.02
Mean IoU (excludes cross-border fires)			0.77 ± 0.08	0.68 ± 0.08	0.76 ± 0.08	0.83 ± 0.09	0.97 ± 0.02

* The IoU for cross-border fires are omitted for FEDS since the perimeter of these fires are not fully mapped

https://doi.org/10.5194/essd-2023-389
Preprint. Discussion started: 27 September 2023

Table C2: Comparison of the final perimeter sinuosity for the 25 non-cross border fires. The sinuosity of the fire perimeter is defined as the length of the perimeter divided by the diameter of a circle with the same area.

Dataset	**Sinuosity** (±1SD)
GOFER-Combined	4.9 ± 1.2
GOFER-East	4.3 ± 0.8
GOFER-West	4.6 ± 0.9
FEDSv2	5.9 ± 1.9
FRAP	14.3 ± 6.7

Table C3: The number of damaged and destroyed structures within GOFER-Combined, GOFER-East, and GOFER-West final perimeters. Undamaged and inaccessible structures are excluded.

#	**Fire Name**	**Year**	**Within Perimeter (%)**			**Total (*n*)**
			GOFER-Combined	GOFER-East	GOFER-West	
5	Creek	2020	95	99	100	840
8	Glass		99	100	100	1066
10	LNU Lightning Complex		91	95	97	1723
11	North Complex		98	98	98	2471
13	SCU Lightning Complex		100	100	100	251
15	SQF Complex		100	100	100	244
18	Antelope	2021	100	100	100	24
19	Beckwourth Complex		100	100	100	171
20	Caldor		100	100	100	1087
21	Dixie		90	91	99	1394
24	McFarland		94	94	100	47
27	Tamarack		100	100	100	17
Mean			97 ± 4	98 ± 3	100 ± 1	

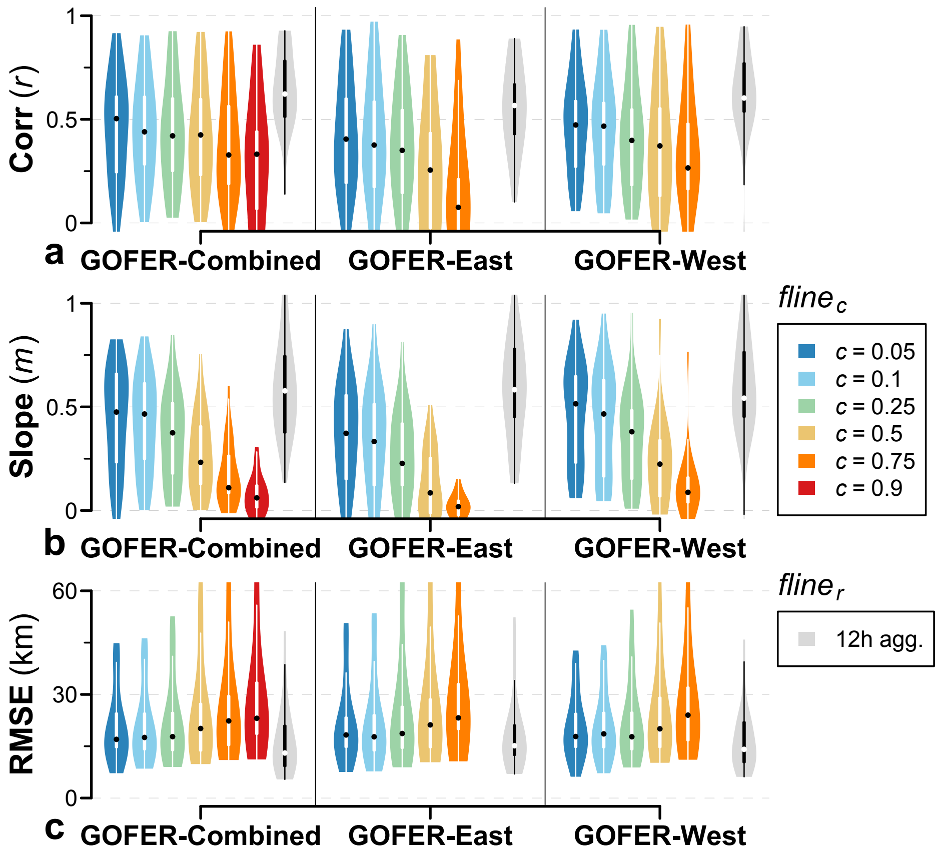

Figure C2: Comparison of GOFER and FEDSv2 active fire line lengths. The violin plots show the distribution of (**a**) correlation coefficients, (**b**) slopes, and (**c**) RMSEs for 25 non-cross border CA fires from 2019-2021. GOFER $fline_c$ lengths are compared to the out-of-box FEDSv2 active fire line lengths, while the 12h aggregate $fline_r$ lengths are calculated using the same method for GOFER and FEDSv2. $fline_{c=0.9}$ was not derived for GOFER-East and GOFER-West as the optimized confidence thresholds used to map perimeters were lower than 0.9.

Table C4: Comparison of GOFER fire spread rates derived from the MAE (maximum axis of expansion) and AWE (area-weighted expansion) methods.

Dataset	**Correlation Coefficient** (r, ±1SD)	**MAE/AWE** (±1SD)
GOFER-Combined	0.93 ± 0.05	2.74 ± 0.12
GOFER-East	0.94 ± 0.02	2.48 ± 0.15
GOFER-West	0.95 ± 0.02	2.56 ± 0.13

https://doi.org/10.5194/essd-2023-389
Preprint. Discussion started: 27 September 2023

Author contribution. TL and JTR designed the study. TL developed the code and carried out the data processing and analysis. All authors contributed to the interpretation of the results. TL prepared the manuscript with contributions from all co-authors.

Competing interests. The authors declare that they have no conflict of interest.

Acknowledgements. TL acknowledges support from the NOAA Climate and Global Change Postdoctoral Fellowship Program, administered by UCAR's Cooperative Programs for the Advancement of Earth System Science (CPAESS) under the NOAA Science Collaboration Program award NA21OAR4310383. JTR acknowledges support from the U.S. DOE Office of Science RUBISCO Science Focus Area and NASA's Modeling Analysis and Prediction (Grant 80NSSC21K1362) program. YC and JTR acknowledge support from the U.S. DOE LLNL-LDRD Program (contract DE-AC52-07NA27344 and project No. 22-ERD-008, "Multiscale Wildfire Simulation Framework and Remote Sensing"). EFG acknowledges support from NASA's Global Precipitation Measuring Mission and Weather and Atmospheric Dynamics (Grants 80NSSC22K0597 and 80NSSC23K1304) and from NSF (IIS 2324008). DCM, JTR., YC, and EBW acknowledge support from NASA's Earth Information System Fire (EIS) project.

Code/Data availability. The code for the GOFER algorithm is available at https://github.com/tianjialiu/gofer. The GOFER dataset of the 28 fires in California from 2019-2021 is available on Zenodo at https://doi.org/10.5281/zenodo.8327265 (Liu et al., 2023). An online data visualization app for the GOFER dataset is available at https://globalfires.earthengine.app/view/gofer.

References

Andela, N., Kaiser, J.W., Van Der Werf, G.R., Wooster, M.J., 2015. New fire diurnal cycle characterizations to improve fire radiative energy assessments made from MODIS observations. Atmos Chem Phys 15, 8831–8846. https://doi.org/10.5194/acp-15-8831-2015

Andela, N., Morton, D.C., Giglio, L., Paugam, R., Chen, Y., Hantson, S., van der Werf, G.R., Randerson, J.T., 2019. The Global Fire Atlas of individual fire size, duration, speed, and direction. Earth Syst Sci Data 11, 529–552. https://doi.org/10.5194/essd-11-529-2019

Archuleta, C.-A.M., Constance, E.W., Arundel, S.T., Lowe, A.J., Mantey, K.S., Phillips, L.A., 2017. The National Map Seamless Digital Elevation Model Specifications, in: Section B, U.S. Geological Survey Standards, of Book 11, Collection and Delineation of Spatial Data. USGS.

Artés, T., Oom, D., de Rigo, D., Durrant, T.H., Maianti, P., Libertà, G., San-Miguel-Ayanz, J., 2019. A global wildfire dataset for the analysis of fire regimes and fire behaviour. Sci Data 6, 296. https://doi.org/10.1038/s41597-019-0312-2

Balch, J.K., Abatzoglou, J.T., Joseph, M.B., Koontz, M.J., Mahood, A.L., McGlinchy, J., Cattau, M.E., Williams, A.P., 2022. Warming weakens the night-time barrier to global fire. Nature 602, 442–448. https://doi.org/10.1038/s41586-021-04325-1

Balch, J.K., St. Denis, L.A., Mahood, A.L., Mietkiewicz, N.P., Williams, T.M., McGlinchy, J., Cook, M.C., 2020. FIRED (Fire Events Delineation): An open, flexible algorithm and database of US fire events derived from the MODIS burned area product (2001–2019). Remote Sens (Basel) 12, 3498. https://doi.org/10.3390/rs12213498

Ben-Haim, Z., Nevo, O., 2023. Real-time tracking of wildfire boundaries using satellite imagery [WWW Document]. URL https://ai.googleblog.com/2023/02/real-time-tracking-of-wildfire.html (accessed 8.25.23).

Burke, M., Driscoll, A., Heft-Neal, S., Xue, J., Burney, J., Wara, M., 2021. The changing risk and burden of wildfire in the United States. Proceedings of the National Academy of Sciences 118, e2011048118. https://doi.org/10.1073/pnas.2011048118

Chen, Y., Hantson, S., Andela, N., Coffield, S.R., Graff, C.A., Morton, D.C., Ott, L.E., Foufoula-georgiou, E., Smyth, P., Goulden, M.L., Randerson, J.T., 2022. California wildfire spread derived using VIIRS satellite observations and an object-based tracking system. Sci Data 9, 249. https://doi.org/10.1038/s41597-022-01343-0

Giglio, L., 2007. Characterization of the tropical diurnal fire cycle using VIRS and MODIS observations. Remote Sens Environ 108, 407–421. https://doi.org/10.1016/j.rse.2006.11.018

Giglio, L., Boschetti, L., Roy, D.P., Humber, M.L., Justice, C.O., 2018. The Collection 6 MODIS burned area mapping algorithm and product. Remote Sens Environ 217, 72–85. https://doi.org/10.1016/j.rse.2018.08.005

Gorelick, N., Hancher, M., Dixon, M., Ilyushchenko, S., Thau, D., Moore, R., 2017. Google Earth Engine: Planetary-scale geospatial analysis for everyone. Remote Sens Environ 202, 18–27. https://doi.org/10.1016/j.rse.2017.06.031

Hall, J.V., Zhang, R., Schroeder, W., Huang, C., Giglio, L., 2019. Validation of GOES-16 ABI and MSG SEVIRI active fire products. International Journal of Applied Earth Observation and Geoinformation 83, 101928. https://doi.org/10.1016/j.jag.2019.101928

Hally, B., Wallace, L., Reinke, K., Jones, S., 2016. Assessment of the utility of the Advanced Himawari Imager to detect active fire over Australia, in: International Archives of the Photogrammetry, Remote Sensing and Spatial Information Sciences - ISPRS Archives. International Society for Photogrammetry and Remote Sensing, pp. 65–71. https://doi.org/10.5194/isprsarchives-XLI-B8-65-2016

Joseph, M.B., Rossi, M.W., Mietkiewicz, N.P., Mahood, A.L., Cattau, M.E., St. Denis, L.A., Nagy, R.C., Iglesias, V., Abatzoglou, J.T., Balch, J.K., 2019. Spatiotemporal prediction of wildfire size extremes with Bayesian finite sample maxima. Ecological Applications 29, e01898. https://doi.org/10.1002/eap.1898

Juang, C.S., Williams, A.P., Abatzoglou, J.T., Balch, J.K., Hurteau, M.D., Moritz, M.A., 2022. Rapid Growth of Large Forest Fires Drives the Exponential Response of Annual Forest-Fire Area to Aridity in the Western United States. Geophys Res Lett 49, e2021GL097131. https://doi.org/10.1029/2021gl097131

Kolden, C.A., 2019. We're not doing enough prescribed fire in the western united states to mitigate wildfire risk. Fire 2, 30. https://doi.org/10.3390/fire2020030

Li, F., Zhang, X., Kondragunta, S., Lu, X., Csiszar, I., Schmidt, C.C., 2022. Hourly biomass burning emissions product from blended geostationary and polar-orbiting satellites for air quality forecasting applications. Remote Sens Environ 281. https://doi.org/10.1016/j.rse.2022.113237

https://doi.org/10.5194/essd-2023-389
Preprint. Discussion started: 27 September 2023

Liu, T., Randerson, J.T., Chen, Y., Morton, D.C., Wiggins, E.B., Smyth, P., Foufoula-Georgiou, E., Nadler, R., Nevo, O., 2023. GOES-Observed Fire Event Representation (GOFER) dataset for 28 California wildfires from 2019-2021. https://doi.org/10.5281/zenodo.8327265

Mu, M., Randerson, J.T., Van Der Werf, G.R., Giglio, L., Kasibhatla, P., Morton, D., Collatz, G.J., Defries, R.S., Hyer, E.J., Prins, E.M., Griffith, D.W.T., Wunch, D., Toon, G.C., Sherlock, V., Wennberg, P.O., 2011. Daily and 3-hourly variability in global fire emissions and consequences for atmospheric model predictions of carbon monoxide. Journal of Geophysical Research: Atmospheres 116, D24303. https://doi.org/10.1029/2011JD016245

Picotte, J.J., Bhattarai, K., Howard, D., Lecker, J., Epting, J., Quayle, B., Benson, N., Nelson, K., 2020. Changes to the Monitoring Trends in Burn Severity program mapping production procedures and data products. Fire Ecology 16, 16. https://doi.org/10.1186/s42408-020-00076-y

Restif, C., Hoffman, A., 2020. How to generate wildfire boundary maps with Earth Engine [WWW Document]. Google Earth and Earth Engine Medium. URL https://medium.com/google-earth/how-to-generate-wildfire-boundary-maps-with-earth-engine-b38eadc97a38 (accessed 6.21.23).

Roberts, G.J., Wooster, M.J., 2008. Fire detection and fire characterization over Africa using Meteosat SEVIRI. IEEE Transactions on Geoscience and Remote Sensing 46, 1200–1218. https://doi.org/10.1109/TGRS.2008.915751

Schmit, T.J., Griffith, P., Gunshor, M.M., Daniels, J.M., Goodman, S.J., Lebair, W.J., 2017. A closer look at the ABI on the GOES-R series. Bull Am Meteorol Soc 98, 681–698. https://doi.org/10.1175/BAMS-D-15-00230.1

Schroeder, W., Csiszar, I., Giglio, L., Ellicott, E., Schmidt, C.C., Hoffman, J.P., Lindstrom, S., 2010. Early characterization of the active fire detection products derived from the next generation NPOESS/VIIRS and GOES-R/ABI instruments. 2010 IEEE International Geoscience and Remote Sensing Symposium. https://doi.org/10.1109/IGARSS.2010.5650863

Spestana, S., Bhushan, S., Carter, J., 2022. spestana/goes-ortho: Initial release (v0.1). Zenodo. https://doi.org/10.5281/zenodo.6455138

van der Werf, G.R., Randerson, J.T., Giglio, L., van Leeuwen, T.T., Chen, Y., Rogers, B.M., Mu, M., van Marle, M.J.E., Morton, D.C., Collatz, G.J., Yokelson, R.J., Kasibhatla, P.S., 2017. Global fire emissions estimates during 1997–2016. Earth Syst Sci Data 9, 697–720. https://doi.org/10.5194/essd-9-697-2017

Wang, S.S.C., Qian, Y., Leung, L.R., Zhang, Y., 2021. Identifying Key Drivers of Wildfires in the Contiguous US Using Machine Learning and Game Theory Interpretation. Earths Future 9, e2020EF001910. https://doi.org/10.1029/2020EF001910

Wiggins, E.B., Soja, A.J., Gargulinski, E., Halliday, H.S., Pierce, R.B., Schmidt, C.C., Nowak, J.B., DiGangi, J.P., Diskin, G.S., Katich, J.M., Perring, A.E., Schwarz, J.P., Anderson, B.E., Chen, G., Crosbie, E.C., Jordan, C., Robinson, C.E., Sanchez, K.J., Shingler, T.J., Shook, M., Thornhill, K.L., Winstead, E.L., Ziemba, L.D., Moore, R.H., 2020. High Temporal Resolution Satellite Observations of Fire Radiative Power Reveal Link Between Fire Behavior and Aerosol and Gas Emissions. Geophys Res Lett 47, e2020GL090707. https://doi.org/10.1029/2020GL090707

Williams, A.P., Abatzoglou, J.T., Gershunov, A., Guzman-Morales, J., Bishop, D.A., Balch, J.K., Lettenmaier, D.P., 2019. Observed impacts of anthropogenic climate change on wildfire in California. Earths Future 7, 892–910. https://doi.org/10.1029/2019EF001210

Xu, W., Wooster, M.J., Roberts, G., Freeborn, P., 2010. New GOES imager algorithms for cloud and active fire detection and fire radiative power assessment across North, South and Central America. Remote Sens Environ 114, 1876–1895. https://doi.org/10.1016/j.rse.2010.03.012

Zhou, X., Josey, K., Kamareddine, L., Caine, M.C., Liu, T., Mickley, L.J., Cooper, M., Dominici, F., 2021. Excess of COVID-19 cases and deaths due to fine particulate matter exposure during the 2020 wildfires in the United States. Sci Adv 7, eabi8789. https://doi.org/10.1126/sciadv.abi878